Perturbation Theory of Large-Particle Diffusion in Liquids

中村, 有花

https://doi.org/10.15017/1543928

Perturbation Theory of Large-Particle Diffusion in Liquids

Yuka Nakamura

Department of Physics,
Graduate School of Science, Kyushu University, Japan

A thesis submitted to Kyushu University
for the degree of doctor of science

September 2015

Abstract

A theoretical study is performed to investigate the effect of the solvation structure on a large-particle diffusion in liquids. The solvation structure stands for the density distribution of solvent particles around the solute. In this thesis, considering the solvation effect, a theory of the translational mobility of a large solute is formulated in one- and two-component solvent systems. The diffusion coefficient is obtained from the drag coefficient through the Einstein relation. Furthermore, using the theory, the diffusion coefficients are calculated numerically to clarify the solvation effect.

First, a theory of the translational mobility in a one-component solvent is formulated by perturbation expansions with respect to the size ratio of the solute and solvent particles. The expansion allows one to derive hydrodynamic equations and boundary conditions on the solute surface up to the first order. Solving the hydrodynamic equations with the boundary conditions, one obtains an analytical expression of the drag coefficient including higher order terms of the size ratio. The drag coefficient can be calculated from the density distribution function. Then, the numerical results of this theory are compared with those calculated by the non-perturbative theory and computer simulation. The numerical results are in good agreement with those of other theories when the size ratio of the solute and solvent particles is larger than 7.

Next, a theory of the drag coefficient in a two-component solvent mixture is formulated by extending the perturbation theory for a one-component solvent system. The drag coefficient is calculated by solving the hydrodynamic equations and boundary conditions on the solute surface. The boundary condition depends on the solvation structure of a binary mixture. Then, to investigate the solvation effects on the diffusion coefficient, the perturbation theory is applied to a binary hard-sphere solvent system. The calculated results show that the diffusion coefficient approaches the value of the Stokes-Einstein relation with the stick boundary condition as adding the larger solvent spheres. The transition to the stick boundary condition is observed when the density of the larger solvent around the solute increases. As the solvent density increases, the velocity of the solvent around the solute approaches zero.

Contents

Chapter 1

Introduction

Diffusion in a liquid is a fundamental phenomenon in biology and chemistry as well as physics.[1]–[14] For instance, proteins move by diffusion in a cell crowded with biomolecules.[15],[16] Since biological phenomena such as protein transport and chemical reaction are often diffusion-limited, many researchers have carried out the study of the diffusion in a liquid to understand biological processes.[1]–[8]

The diffusion of a macroscopic particle, such as a colloidal particle can be described well by the Stokes-Einstein (SE) relation.[17],[18] It is the combination of the Einstein relation and Stokes law. Through the Einstein relation, the diffusion coefficient is related to the translational mobility of the solute particle. The Stokes law gives the drag coefficient, which depends on the viscosity of the solvent, the radius of the solute, and the boundary condition on the solute surface. Since the Stokes law is derived from the hydrodynamic equations, its validity is limited to macroscopic particles.

Recently, much attention has been paid to the effect of the solvation structure around the solute. Terazima and co-workers have observed the solvation effect on the diffusion coefficient in the folding of the protein.[1]–[3] They showed that the diffusion coefficient nearly doubles when the hydration structure is destroyed during the protein folding process. Since this solvation effect is not included in the Stokes law, it causes the breakdown of the Stokes law.

The breakdown of the Stokes law has been observed in other experiments of the solute smaller than macroscopic size.[5]–[10],[19],[20] In particular, the large deviation from the SE relation has been found in the experiments of the diffusion in a multi-component solvent mixture system.[5]–[8] However, there is little understanding of the relation between the solvation effects and the breakdown of the Stokes law.

It is difficult to study the solvation effect on a large-particle diffusion using microscopic theories[21]–[27] or computer simulations,[28]–[38] because of the finite-size

effect.[28],[39] In simulation studies, since the diffusion coefficient depends on the size of the simulation cell, one cannot obtain the diffusion coefficient of a solute in the infinite system. As is the case of the simulations, the microscopic theories cannot take account of the solvent particles at an infinite distance because the calculation region is finite when solving equations numerically. To avoid this difficulty, Inayoshi *et al.* have formulated a theory by perturbation expansions with respect to the size ratio of the solute and solvent particles.[40] Their theory, however, gives the drag coefficient much larger than those obtained by the non-perturbative theory.[26] Furthermore, the application of their theory is limited to the one-component solvent system. There are few theoretical studies for the diffusion in mixtures.

The purpose of this thesis is to clarify the solvation effect on the diffusion coefficient of a large particle. I formulate a theory on the basis of the theory formulated by Inayoshi *et al.*, considering the higher-terms of the perturbation expansion. I show that the numerical results of the theory are in good agreement with those of the simulations and previous theory. In addition, I formulate the theory for the drag coefficient in a binary mixture, extending the perturbation theory for a one-component solvent system. Applying the theory to the binary-hard sphere system, I show that the diffusion coefficient changes from the SE relation with the slip boundary condition to the stick boundary condition due to the solvation effect.

This thesis is organized as follows. In chapter 2, I review previous studies of experiments, MD simulations, and theories for a large-particle diffusion. In chapter 3, I explain the perturbation theory developed by Inayoshi *et al.* In chapter 4, I formulate a theory on the basis of the theory developed by Inayoshi *et al.* The calculated results of this theory are compared with those obtained by the previous theory and MD simulation. In chapter 5, I formulate a theory of the diffusion in the two-component solvent system. I apply the theory to binary hard-sphere systems in chapter 6. In chapter 7, I present the conclusion of this thesis.

Chapter 2

Review of large-particle diffusion

2.1 Stokes-Einstein relation

In the case of a macroscopic spherical solute, the translational diffusion coefficient is described by the combination of the Einstein relation and Stokes law. The Einstein law shows that the diffusion coefficient D is related to the drag coefficient ξ of the solute particle as[41]

$$D = \frac{k_B T}{\xi} \tag{2.1}$$

where k_B is the Boltzmann constant and T is the temperature. Equation (2.1) is a form of the fluctuation-dissipation theorem in the Brownian motion. This relation holds regardless of the size of the solute particle.

The Stokes law gives the drag coefficient based on the hydrodynamic approach. The drag coefficient is calculated by the drag force exerted on the fixed solute particle by the steady solvent flow. The solvent flow has a small velocity $\mathbf{u}$ at an infinite distance from the solute. According to the incompressible hydrodynamic equations, the dynamics of solvent flow is described as follows:[17],[18]

$$\nabla \cdot \mathbf{v}(\mathbf{r}) = 0, \tag{2.2}$$

$$-\nabla P(\mathbf{r}) + \eta \nabla^2 \mathbf{v}(\mathbf{r}) = 0. \tag{2.3}$$

Here, $\mathbf{v}(\mathbf{r})$ is the velocity, $P(\mathbf{r})$ is the pressure, and η is the shear viscosity. Equation (2.2) is the continuity equation and Eq. (2.3) is the linearized Navier-Stokes equation.

To solve above equations, the boundary condition is required at the solute surface. The solvent velocity normal to the solute surface is assumed to be zero, that is,[17],[18]

$$v_r(\mathbf{r}) = 0, \tag{2.4}$$

where $v_r(\mathbf{r})$ is the r component of $\mathbf{v}(\mathbf{r})$ in the spherical coordinates. The origin of the coordinate system is the center of the solute particle and the z-axis corresponds to the $\mathbf{u}$ direction. Then, the ϕ component of $\mathbf{v}(\mathbf{r})$ is zero, that is, $v_\phi(\mathbf{r}) = 0$.

The solvent velocity tangent to the solute surface has been typically assumed to obey the stick boundary condition or slip boundary condition.[17], [18] The stick boundary condition is given as

$$v_\theta(\mathbf{r}) = 0, \tag{2.5}$$

where $v_\theta(\mathbf{r})$ is the θ component of $\mathbf{v}(\mathbf{r})$ in the spherical coordinates. The velocity is assumed to be zero at the solute surface. The slip boundary condition is given as

$$\frac{dv_\theta(\mathbf{r})}{dr} - \frac{v_\theta(\mathbf{r})}{r} = 0. \tag{2.6}$$

The left hand side corresponds to the tangential component of the force on an element of the solute surface. In the slip boundary condition, the velocity has a finite value at the solute surface.

Solving Eqs. (2.2) and (2.3) under the boundary condition at the solute surface, one can derive the drag force as $\mathbf{F} = \xi\mathbf{u}$. The drag coefficient ξ is obtained as

$$\xi = c\pi\eta R, \tag{2.7}$$

where R is the radius of the solute particle. The parameter c depends on the boundary condition where the stick boundary condition gives $c = 6$, and the slip boundary condition gives $c = 4$.

The combination of Eqs. (2.1) and (2.7) is called the Stokes-Einstein (SE) relation. The application of the SE relation is limited to the macroscopic solute particles since the Stokes law is derived using the hydrodynamics. The solute particle has to be large enough to treat the solvent as a continuum.

2.2 Experimental studies

2.2.1 Breakdown of Stokes law

The validity of the SE relation has been studied in experimental studies.[1]–[14], [19], [20] It is well known that the SE relation can describe the experimental results of the macroscopic particle, such as a colloidal sphere.[12] In contrast, the breakdown of the Stokes law has been observed in some experiments on the diffusion of the solute smaller than the macroscopic size.[5]–[10], [19], [20]

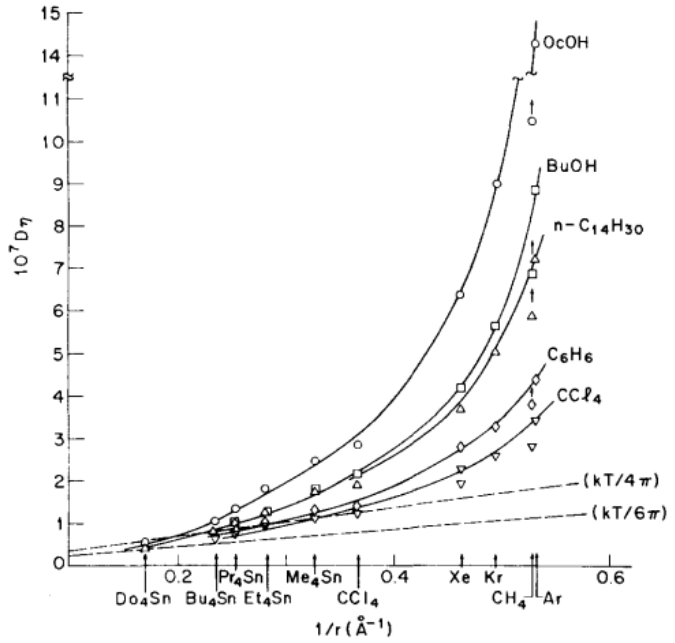

Figure 2.1 Comparison of the diffusion coefficient D of the solutes in various solvents with the prediction of the SE relation.[20] Here, η is the viscosity and r is the radius of the solute. The dotted lines show the predictions of the SE relation for the stick boundary condition $(1/6\pi)$ and slip boundary condition$(1/4\pi)$, respectively.

Evans *et al.* have investigated the diffusion coefficient of the solute particles of various sizes in alcohols, hydrocarbons, and carbon tetrachloride.[19],[20] The diffusion coefficients were determined with the Taylor dispersion technique.[42] In this method, a dilute solution pulse of the solute is injected in a laminar flowing stream of the solvent. The solute is dispersed by the laminar flow and diffusion. The diffusion coefficient is evaluated from the distribution of the solute.

They found that the diffusion coefficient deviates from the SE relation with decreasing the solute size. In Fig. 2.1, the diffusion coefficient-viscosity product $D\eta$ is plotted as a function the inverse of the solute radius $1/r$. If the SE relation holds, $D\eta$ is proportional to $1/r$. For the larger solutes, such as tetrabutyltin and tetradodecyltin, the diffusion coefficient is close to the value predicted by the SE relation. However, the deviation from the SE relation increases as the solute size decreases. This behavior was observed in all solvents.

Some studies have indicated that the breakdown of the Stokes law depends on the interaction between solute and solvent particles.[9],[10] Castillo *et al.* have measured the diffusion coefficient of C_{60} in toluene, benzene, and carbon tetrachloride by the

Table 2.1 The hydrodynamic diameters of C_{60} in the solvents.[9] The diameters d_{stick} and d_{slip} are evaluated from the diffusion coefficient using the SE relation for the stick and slip boundary conditions, respectively. The X-ray studies reported that the diameter of C_{60} is 7.1Å.[43]

system	d_{stick}(Å)	d_{slip}(Å)
C_{60}/toluene	8.72 ± 0.32	13.08 ± 0.48
C_{60}/benzene	3.30 ± 0.04	4.94 ± 0.06
C_{60}/CCl_4	6.56 ± 1.02	9.86 ± 1.53

Taylor dispersion technique.[9] In solution, the size and shape of C_{60} change little with the solvents in contrast with other solutes.[9] From the obtained diffusion coefficient and the viscosity of the solvent, they calculated the hydrodynamic diameter $d = 2R$ using the SE relation (Table 2.1). If the Stokes law folds, the hydrodynamic diameter does not change depending on the solvent. However, the calculated diameters are different depending on the solvent. It can be considered that the diffusion coefficients reflect the difference of the solute-solvent interactions.

2.2.2 Effects of solvation structure

In recent years, much attention has been paid to the effects of the solvation structure on the diffusion coefficient.[1]–[3] The solvation structure around the solute is determined by the solute-solvent and solvent-solvent interactions. Terazima and coworkers have observed the diffusion coefficient during the protein folding process, by which the protein forms its functional three-dimensional structure.[1]–[3] They investigated the relationship between the diffusion coefficient and the protein conformations for cytochrome *c*.

To determine the diffusion coefficient, they used the transient grating technique.[44] In this measurement, the solute in the sample is photoexcited with interference pattern by two laser beams to induce the refractive index modulation in the sample. This modulation is monitored by the diffracted light of the prove beam entering in the sample (TG signal). Since the signal decays by the diffusion of the solute, one can obtain the diffusion coefficient from the decay of the TG signal.

Terazima *et al.* have found that the diffusion coefficient increases 1.9 times at 41ms after the start of the folding process. According the studies using the circular dichroism experiments,[45] the size of cytochrome *c* changes little at this time. In contrast, the hydration structure changes around cytochrome *c* when the diffusion

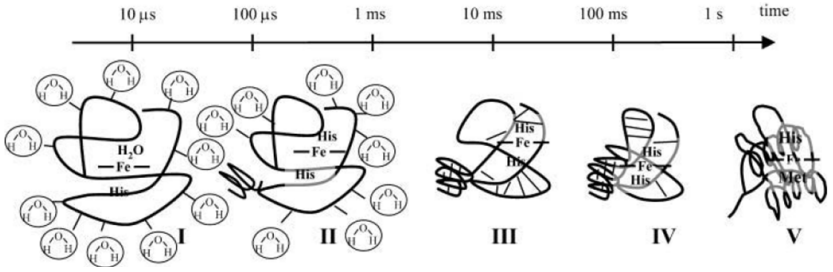

Figure 2.2 Schematic illustrations of the folding dynamics of cytochrome *c*:[1] (I) unfolded cytochrome *c*; (II) a small amount of a-helix is formed; (III) hydrogen bonding is rearranged from the intermolecular one between the protein and solvent to the intramolecular one; (IV) formation of the α-helix in the major part; (V) native cytochrome *c*. The thick lines indicate the protein backbone and the thin lines represent the hydrogen bonding.

coefficient increases (Fig. 2.2 III). The hydrogen bonding is rearranged from the intermolecular one between the protein and solvent to the intramolecular one to form the α-helix formation.

Their results show that the diffusion coefficient reflects not only the size of the protein but also the hydration structure. The diffusion coefficient is small when the density of solvent molecules is high around the protein. Then, the protein molecule feels more drag force from the water molecules.

2.2.3 Studies of diffusion in mixture

The validity of the Stokes law has also been studied in experiments of a protein diffusion in a multicomponent solvent mixture.[4]–[8] The proteins diffuse in a cell crowded with biomolecules including nucleic acids, glucides, and lipids. Thus, to understand the diffusion of a protein in vivo, many researchers have carried out in vitro experiments on the diffusion in a solvent mixture.[5]–[8] Some experiments of them showed the large deviation from the SE relation in a solvent mixture system.[5]–[8]

Zorrilla *et al.* have obtained the diffusion coefficient of apomyoglobin in a protein crowded environment by using the fluorescence correlation spectroscopy.[6] They measured the fluctuations in the fluorescence intensity of the diffusing molecules in an open sample volume, which is produced by a focused laser and confocal optics. The fluctuations are caused by the diffusion of the fluorescent molecules into or out of the open sample volume. The autocorrelation analysis of the fluctuations provides the diffusion coefficient of the fluorescence.

Figure 2.3 shows the diffusion coefficient and viscosity as a function of the concen-

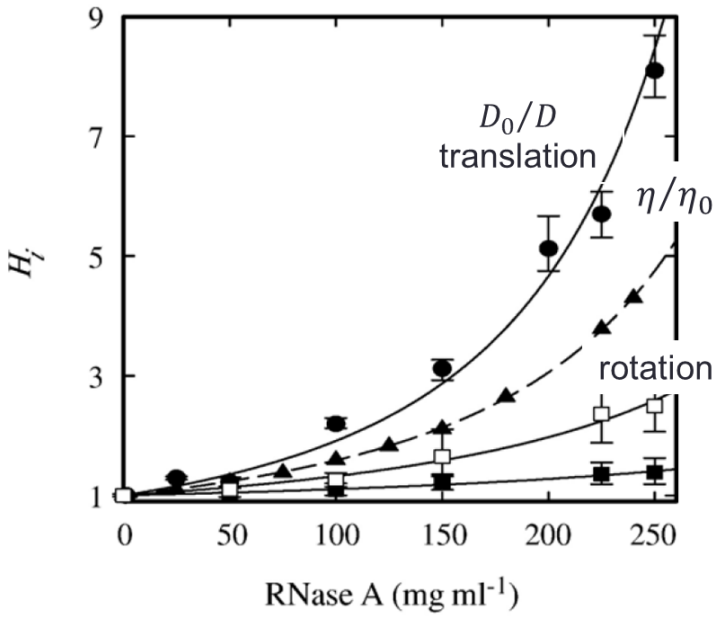

Figure 2.3 Translational (circles) and rotational (squares) diffusion coefficients of apomyoglobin and the viscosity (triangles) relative the values for the infinitely dilute solution of ribonuclease A.[6] All translational diffusion data correspond to apomyoglobin monomer. Filled and Open squares correspond to the overall motion of apomyoglobin dimer, and to a combination of the global motion of apomyoglobin monomer and the librational motions of apomyoglobin dimer, respectively. I added the description of the symbols to the original figure.

tration of crowding molecules, ribonuclease A. When the Stokes law folds, one can derive $D_0/D = \eta/\eta_0$ where D_0 and η_0 are the diffusion coefficient and viscosity for the infinitely dilute solution of ribonuclease A. However, the ratio D_0/D deviates from η/η_0 as the concentration of ribonuclease A increases. Since $D_0/D > \eta/\eta_0$, D has a value smaller than the value predicted by the SE relation. These results indicate that the diffusion coefficient cannot be explained only by the viscosity of a mixture.

These deviations have been observed in experiments of other proteins, such as a dUTPase in a disaccharide solution[7] and a phototropin in the ficoll solutions.[5] Furthermore, the breakdown of the Stokes law has also been found in the diffusion of colloidal spheres in polymer solutions.[13],[14] Some researchers consider that the deviation is caused by the solvation structure around the solute.[14] The origin of the breakdown in a solvent mixture system, however, has not been fully understood.

2.3 Simulation studies

2.3.1 Solute size dependence

The solute size dependence of the diffusion coefficient has been well studied using molecular dynamics (MD) simulation[28]–[35] since it is easy to change the solute size in contrast to experimental studies. The researchers have carried out the MD simulations to determine the critical size above which the SE relation holds, and the boundary condition on the solute surface.[28]–[34]

Sokolovskii *et al.* have carried out the MD simulation of hard sphere systems to study the size dependence of the solute particle diffusion.[28] The system composed a single solute with the diameter Σ and N-1 solvent particles with the diameter σ in the cubic cell of length L of the periodic boundary condition. The diffusion coefficients were determined using the Green-Kubo relation,[46], [47]

$$D = \frac{1}{3}\int_0^\infty \langle \boldsymbol{u}(t) \cdot \boldsymbol{u}(0) \rangle \, dt, \tag{2.8}$$

which is equivalent to the Einstein expression,[46]

$$D = \frac{1}{6}\lim_{t\to\infty}\frac{d}{dt}\left\langle |\boldsymbol{r}(t) - \boldsymbol{r}(0)|^2 \right\rangle. \tag{2.9}$$

Here, $\boldsymbol{r}(t)$ and $\boldsymbol{v}(t)$ are the position and velocity of the solute particle.

They showed that the calculated results suffer from the finite size effect. Figure 2.4 shows the dependence of the diffusion coefficient on the simulation cell length L. The diffusion coefficient D_N becomes smaller with the reciprocal cell length L^{-1}. Here, D_N denotes the diffusion coefficent obtained from a simulation with N particles. At the constant number density, $N \propto L^3$.

The finite size effect arises from the long-range effect of the solute particle on solvent particles due to the momentum conservation.[28], [39] Thus, the calculation of the diffusion coefficient requires a large system which includes many solvent particles. However, since the simulation cell is finite, there is the hydrodynamic interactions between the tracer particle and its images resulting from the periodic boundary conditions. The finite size effect increases with the size of a large solute particle. Thus, the diffusion coefficient of a large solute particle in the infinite system cannot be obtained directly by computer simulations.

Sokolovskii *et al.* evaluated the diffusion coefficient in the infinite simulation cell D_∞ using a linear extrapolation of results obtained from the finite system D_N as

$$\frac{D_N}{D_{slip}} = \frac{D_\infty}{D_{slip}} - k\frac{R}{L}. \tag{2.10}$$

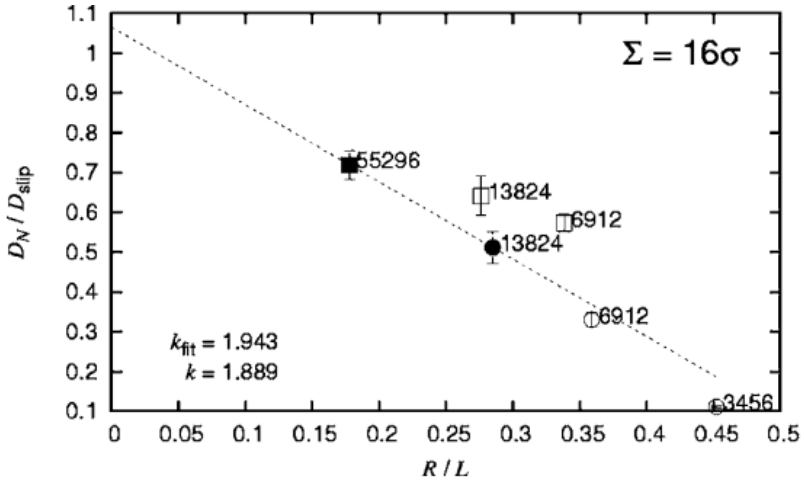

Figure 2.4 Dependence of the diffusion coefficient D_N on the length of the simulation cell L.[28] Labels at the symbols show the number of particles in the simulation cell. The circles and squares are simulation results without and with volume correction, respectively. They adjusted the cell volume to keep the solvent density constant when the solute particle is immersed in the cell. The filled symbols are the results used in a linear least squares fitting routine to determine the fitted slope k_{fit}. Here, the slope k in Eq. (2.10) is the value calculated by the Fushiki's formula. The diameter of the solute particle is 16σ where σ is the diameter of the solvent particle. The density of solvent particles is $\rho\sigma^3 = 0.52$.

Here, D_{slip} is the value calculated from the SE relation with the slip boundary condition, and the effective radius is defined as $R = (\Sigma+\sigma)/2$ where the solvent particle cannot approach the solute particle for $r < R$. The diffusion coefficient D_N is assumed to be linear in the reciprocal cell length L^{-1} with the slope k. They obtained k using the Fushiki's formula which takes account of the hydrodynamic interactions.[39] It is calculated from the kinematic viscosity and the diffusion coefficient obtained by the kinetic theory using the method of Enskog.[48]–[51]

Figure 2.5 shows the dependence of the diffusion coefficient on the effective radius. The results with extrapolation lie close the value of the SE relation with slip boundary condition for $R/\sigma \geq 3$. Note that the results without extrapolation approaches the stick boundary condition. The difference of the results obtained with and without extrapolation increases as the solute becomes large. These results show the importance of considering the finite size effect.

The solute size dependence has been studied in other interaction systems than the hard-sphere. As is the case of the hard-sphere system, the SE relation with the

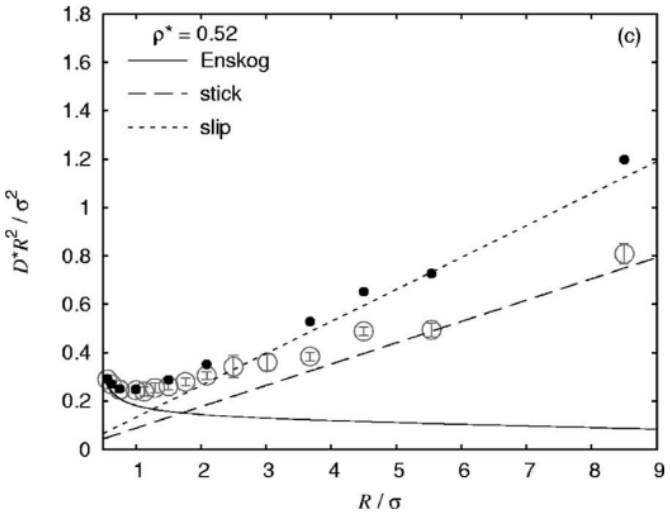

Figure 2.5 Dependence of the diffusion coefficient $D^* = D(m/k_B\sigma^2)^{1/2}$ on the effective radius $R = (\Sigma + \sigma)/2$.[28] Open and filled symbols are the results obtained without and with extrapolation. The solid line represents the Enskog result, and the long and short dashed lines represents the SE relation with with stick and slip boundary conditions, respectively. These are calculated using the effective radius instead of the solute radius. The density of solvent particles is $\rho\sigma^3 = 0.52$.

slip boundary condition was also observed for a large solute when the solute-solvent interaction is purely repulsive, such as repulsive Weeks-Chandler-Andersen (WCA) potentials.[29] In addition, when the interaction includes a weak attraction, the boundary condition approached the SE relation with the slip condition as the solute size increases.[31],[33],[34] In contrast, when the solute surface is rough, the diffusion coefficient approached the SE relation with the stick boundary condition.[29],[37] Most studies have not determined the critical size, above which the SE relation holds. The large solute was not treated because of the finite size effect.

2.3.2 Effects of solute-solvent interaction

As shown in experimental studies, a large particle diffusion depends on the interparticle interactions. Thus, many MD simulation studies have carried out to examine the effect of the solute-solvent interaction.[29],[32],[34],[36] Schimit *et al.* have studied the effect of the solute-solvent attractive interaction on the diffusion coefficient by the MD simulation.[29] The diffusion coefficients were calculated using the Green-Kubo relation Eq. (2.8).

The interaction between solvent particles was assumed as the Lennard-Jones po-

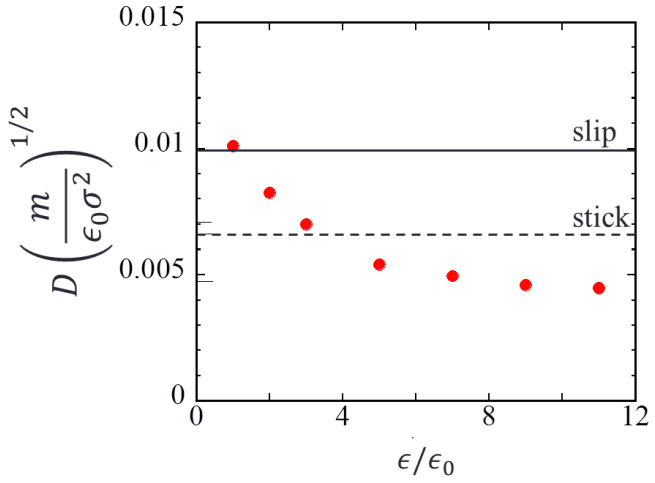

Figure 2.6 Dependence of the diffusion coefficient D on the strength of the solute-solvent attractive interaction ϵ. I plotted the diffusion coefficients obtained by Schimit *et al.*[29] Solid and dashed lines represent the value predicted by the SE relation with the stick and slip boundary conditions, respectively. These are calculated using the effective hydrodynamic radius $a+\sigma$. The density of solvent particles is $\rho\sigma^3 = 0.85$.

tential, where the energy and length parameters are ϵ_0 and σ, respectively. The solute-solvent interaction was given by

$$u(r) = 4\epsilon \left[\left(\frac{\sigma}{r-a} \right)^{12} - \left(\frac{\sigma}{r-a} \right)^{6} \right] S(r-a) \tag{2.11}$$

where the switching function $S(r)$ is 1 for $r < r_1$,

$$S(r) = (r_2^2 - r^2)^2 (r_2^2 + 2r^2 - 3_1^2)/(r_2^2 - r_1^2)^3 \tag{2.12}$$

for $r_1 < r < r_2$, and zero for $r > r_2$. The strength of the attractive interaction is represented by the well depth ϵ at $r = r_1$ in Eq. (2.11). They employed $r_1 = 2^{1/6}\sigma$ and $r_2 = 3\sigma/2$. In addition, they assumed that the radii of the solute and solvent particles are $a + \sigma/2$ and $\sigma/2$, respectively. In this simulation, $(a+\sigma/2)^3/(\sigma/2)^3 = 100$.

As the attractive force increases, the diffusion coefficient changes from the SE relation with the slip condition to that with the stick condition (Fig. 2.6). When the attractive interaction is weak, the result has the value close to the SE relation with the slip boundary condition. Here, the SE relation was calculated using the effective radius $R_a = a + \sigma$ instead of the solute radius. As increasing the attractive

interaction, the diffusion coefficient decreases. The results converge to the value smaller than the SE relation with the stick boundary condition. They showed that this value is almost the same as the SE relation with the stick boundary condition calculated using the corrected effective radius $R_a = a + (1 + \sigma^{1/6})$. They evaluated this radius considering a solvation shell caused by the strong attraction between solute and solvent particles. The particles in the solvation shell are assumed to sit directly at the potential minimum of the solute-solvent interaction, which is at $a + 2^{1/6}\sigma$.

The transition of the boundary condition has observed in some studies of the attractive interaction effect.[29],[32],[34] Researches have pointed out that the stick condition is related to the accumulation of solvent particles around the solute due to the attractive force.[29],[32]

2.4 Theoretical studies

The SE relation is not valid for the solute particle smaller than the macroscopic size because the Stokes law is derived from hydrodynamic equations. Actually, the breakdown of the Stokes law has been observed in experiments and simulation studies as shown above. The breakdown arises because the diffusion coefficient is affected by the interparticle interactions, which in not considered in the Stokes law. To treat a large particle, such as a protein, one needs the microscopic theory including the effects of the interparticle interactions.

The calculation of the drag coefficient requires the dynamics of the solvent around the solute particle. In previous theories, the dynamics was approximated by that of the neat solvent[52]–[56] although the dynamics near the solute is much affected by the solute-solvent interaction. To address this problem, Yamaguchi *et al.* have formulated the inhomogeneous generalized Langevin equations.[26] Using their theory, one can calculate the drag coefficient, considering the solute-solvent and solvent-solvent interactions.

2.4.1 Generalized Langevin equations

They considered the system composed of N solvent particles of the mass m. The position and momentum of particle i are denoted by $\boldsymbol{r}_i$ and $\boldsymbol{p}_i$, respectively. The time development of $\boldsymbol{r}_i$ and $\boldsymbol{p}_i$ obey the Hamiltonian dynamics where $\mathcal{H}$ is the hamiltonian of the system. The interaction between the solute and solvent particles is regarded as the external field $u(\mathbf{r})$ applied to the solvent particles.

Yamaguchi *et al.* formulated the generalized Langevin equations for the time development of the conserved quantities, the density field $\rho(\boldsymbol{r})$ and current density field $\boldsymbol{J}(\boldsymbol{r})$ under the external field. These quantities are defined as

$$\rho(\boldsymbol{r}) \equiv \sum_i \delta(\boldsymbol{r} - \boldsymbol{r}_i) \tag{2.13}$$

$$\boldsymbol{J}(\boldsymbol{r}) \equiv \sum_i \boldsymbol{v}_i \delta(\boldsymbol{r} - \boldsymbol{r}_i). \tag{2.14}$$

Here, $\mathbf{v}_i$ is the velocity of particle i. The generalized Langevin equations are derived from the Liouville equations using the projection operator method.[57]

Liouville equation

The time developments of $\rho(\boldsymbol{r})$ and $\boldsymbol{J}(\boldsymbol{r})$ are represented by the exact equation using the Liouville operator $\mathcal{L}$ as[46]

$$\frac{\mathrm{d}X_\mu}{\mathrm{d}t} = i\mathcal{L}X_\mu, \quad i\mathcal{L} \equiv \sum_i \left\{ \frac{\partial \mathcal{H}}{\partial \boldsymbol{p}_i} \cdot \frac{\partial}{\partial \boldsymbol{r}_i} - \frac{\partial \mathcal{H}}{\partial \boldsymbol{r}_l} \cdot \frac{\partial}{\partial \boldsymbol{p}_l} \right\} \tag{2.15}$$

where $\{X_\mu\} = \{\rho, \boldsymbol{J}\}$. Equation (2.15) is solved formally as

$$X_\mu(t) = e^{i\mathcal{L}t} X_\mu(0). \tag{2.16}$$

Then, the time development of $X_\mu(t)$ is given as

$$\frac{\mathrm{d}X_\mu}{\mathrm{d}t} = e^{i\mathcal{L}t} i\mathcal{L}X_\mu(0). \tag{2.17}$$

Projection operator method

Using the projection operator method,[46],[57]–[59] one derives the generalized Langevin equation, which is also an exact equation. By the projection operator method, the time development of $\{X_\mu\}$ is separated into slowly-varying and quickly-varying parts.

To separate the slowly-varying parts, one projects all phase functions $\{X_\mu\}$ into the subspace defined by a set of slow variables $\boldsymbol{A} = \{A_\mu\}$. Yamaguchi *et al.* chose the conserved variables $\boldsymbol{A} = \{\delta\rho(\boldsymbol{r}), \boldsymbol{J}(\boldsymbol{r})\}$ as the subspace. The projection of X_μ onto $\boldsymbol{A}$ is written by the projection operator $\mathcal{P}$ as

$$\mathcal{P}X_\mu \equiv \sum_{\nu,\lambda} \iint \mathrm{d}\boldsymbol{r}'\mathrm{d}\boldsymbol{r}'' \langle X_\mu(\boldsymbol{r}) A_\nu(\boldsymbol{r}') \rangle \langle \boldsymbol{A}(\boldsymbol{r}'), \boldsymbol{A}(\boldsymbol{r}'') \rangle^{-1}_{\nu\lambda} A_\lambda(\boldsymbol{r}'') \tag{2.18}$$

where $\langle \boldsymbol{A}, \boldsymbol{A} \rangle^{-1}$ represents inverse matrix of the matrix $\langle \boldsymbol{A}, \boldsymbol{A} \rangle$. The element $\nu\mu$ of the matrix is $\langle A_\nu A_\mu \rangle$. Here, the bracket denotes the equilibrium ensemble average of the function as

$$\langle Y(\boldsymbol{r}) Z(\boldsymbol{r'}) \rangle \equiv \int Y(\boldsymbol{r}) X(\boldsymbol{r'}) f_{eq}(\{\boldsymbol{r}^N, \boldsymbol{p}^N\}) \mathrm{d}\boldsymbol{r}^N \mathrm{d}\boldsymbol{p}^N, \tag{2.19}$$

where $f_{eq}(\{\boldsymbol{r}^N, \boldsymbol{p}^N\})$ represents the phase-space probability density. At $|\boldsymbol{r}_i| \to \infty$ and $|\boldsymbol{p}_i| \to \infty$, $f_{eq}(\{\boldsymbol{r}^N, \boldsymbol{p}^N\}) \to 0$. In addition, one defines the operator $\mathcal{Q} \equiv 1 - \mathcal{P}$ projecting onto the subspace orthogonal to $\boldsymbol{A}$.

Using the operator $\mathcal{P}$ and $\mathcal{Q}$, Eq. (2.17) is rewritten as

$$\frac{\mathrm{d}X_\mu}{\mathrm{d}t} = e^{i\mathcal{L}t} i\mathcal{L} X_\mu = e^{i\mathcal{L}t} \mathcal{P} i\mathcal{L} X_\mu + e^{i\mathcal{L}t} \mathcal{Q} i\mathcal{L} X_\mu. \tag{2.20}$$

Here, one wrote $X_\mu(0)$ as X_μ for simplicity.

The first term of the right hand side in Eq. (2.20) is rewritten using Eq. (2.18) as

$$\begin{aligned} e^{i\mathcal{L}t} \mathcal{P} i\mathcal{L} X_\mu &= e^{i\mathcal{L}t} \sum_{\nu,\lambda} \iint \mathrm{d}\boldsymbol{r'} \mathrm{d}\boldsymbol{r''} \langle (i\mathcal{L} X_\mu) A_\nu \rangle \langle \boldsymbol{A}, \boldsymbol{A} \rangle^{-1}_{\nu\lambda} A_\lambda \\ &= \sum_{\nu,\lambda} \iint \mathrm{d}\boldsymbol{r'} \mathrm{d}\boldsymbol{r''} \langle (i\mathcal{L} X_\mu) A_\nu \rangle \langle \boldsymbol{A}, \boldsymbol{A} \rangle^{-1}_{\nu\lambda} A_\lambda(t) \equiv \sum_{\lambda} \iint \mathrm{d}\boldsymbol{r'} \mathrm{d}\boldsymbol{r''} i\Omega_{\mu\lambda} A_\lambda(t). \end{aligned} \tag{2.21}$$

Here, $i\Omega_{\mu\lambda} \equiv \sum_\nu \langle (i\mathcal{L} A_\mu) A_\nu \rangle \langle \boldsymbol{A}, \boldsymbol{A} \rangle^{-1}_{\nu\lambda}$. To derive Eq. (2.21), one used that $i\Omega_{\mu\lambda}$ does not include $\{\boldsymbol{r}^N, \boldsymbol{p}^N\}$.

The second term of the right hand side in Eq. (2.20) is rewritten using the relation derived by Mori,[57]

$$e^{i\mathcal{L}t} = \int_0^t e^{i\mathcal{L}t'} \mathcal{P} i\mathcal{L} e^{\mathcal{Q} i\mathcal{L}(t-t')} \mathrm{d}t' + e^{\mathcal{Q} i\mathcal{L} t}. \tag{2.22}$$

Then, one can obtaine

$$\begin{aligned} e^{i\mathcal{L}t} \mathcal{Q} i\mathcal{L} X_\mu &= \int_0^t e^{i\mathcal{L}t'} \mathcal{P} i\mathcal{L} e^{\mathcal{Q} i\mathcal{L}(t-t')} \mathcal{Q} i\mathcal{L} X_\mu \mathrm{d}t' + e^{\mathcal{Q} i\mathcal{L} t} \mathcal{Q} i\mathcal{L} X_\mu \\ &= \int_0^t e^{i\mathcal{L}t'} \mathcal{P} i\mathcal{L} R_\mu(t-t') \mathrm{d}t' + R_\mu(t) \end{aligned} \tag{2.23}$$

where $R_\mu(t) \equiv e^{\mathcal{Q} i\mathcal{L} t} \mathcal{Q} i\mathcal{L} X_\mu$.

Substituting Eq. (2.18) into the first term of the right hand side in Eq. (2.23), one derives

$$\int_0^t e^{i\mathcal{L}t'} \mathcal{P} i\mathcal{L} R_\mu(t-t') \mathrm{d}t' = \int_0^t \mathrm{d}t' \sum_{\nu,\lambda} \iint \mathrm{d}\boldsymbol{r'} \mathrm{d}\boldsymbol{r''} \langle (i\mathcal{L} R_\mu(t-t')) A_\nu \rangle \langle \boldsymbol{A}, \boldsymbol{A} \rangle^{-1}_{\nu\lambda} A_\lambda(t'). \tag{2.24}$$

From the definition of the bracket Eq. (2.19) and using partial integration, one can derive

$$\langle (i\mathcal{L}R_\mu(t))A_\nu\rangle = -\langle R_\mu(t)(i\mathcal{L}A_\nu)\rangle = -\langle R_\mu(t)\dot{A}_\nu\rangle \tag{2.25}$$

In addition, since $R_\mu(t)$ is normal to the subspace $\{A_\mu\}$, $\langle R_\mu(t)A_\nu\rangle = 0$. Then, one obtains

$$-\langle R_\mu(t)\dot{A}_\nu\rangle = -\langle R_\mu(t)\mathcal{Q}\dot{A}_\nu\rangle = -\langle R_\mu(t)R_\nu\rangle. \tag{2.26}$$

From Eqs.(2.25) and (2.26), Eq. (2.24) is written by

$$\int_0^t e^{i\mathcal{L}t'}\mathcal{P}i\mathcal{L}R_\mu(t-t')\mathrm{d}t' = -\sum_\lambda \int_0^t \mathrm{d}t' \iint \mathrm{d}\boldsymbol{r'}\mathrm{d}\boldsymbol{r''}M_{\mu\lambda}(t-t')A_\lambda(t') \tag{2.27}$$

where

$$M_{\mu\lambda}(t) = \sum_\nu \langle R_\mu(t)R_\nu\rangle\langle \boldsymbol{A},\boldsymbol{A}\rangle^{-1}_{\nu\lambda}. \tag{2.28}$$

Substituting Eqs. (2.21), (2.23), and (2.27) into Eq. (2.20), one derives the generalized Langevin equation,

$$\frac{\mathrm{d}X_\mu}{\mathrm{d}t} = \sum_\lambda \iint \mathrm{d}\boldsymbol{r'}\mathrm{d}\boldsymbol{r''}i\Omega_{\mu\lambda}A_\lambda(t) - \sum_\lambda \int_0^t \mathrm{d}t' \iint \mathrm{d}\boldsymbol{r'}\mathrm{d}\boldsymbol{r''}M_{\mu\lambda}(t-t')A_\lambda(t') + R_\mu(t). \tag{2.29}$$

The first term is proportional to $\boldsymbol{A}$ at the present time. The second term is called the Memory term proportional to $\boldsymbol{A}$ in the past. The third term represents the random force, which is orthogonal to $\boldsymbol{A}$.

Dynamics of solvent particles

Substituting $\{A_\mu\} = \{\rho, \boldsymbol{J}\}$ into Eq. (2.29), Yamaguchi *et al.* derived the time development of $\{X_\mu\} = \{\rho, \boldsymbol{J}\}$ as follows:[26]

$$\frac{\mathrm{d}\rho(\boldsymbol{r},t)}{\mathrm{d}t} = -\nabla\cdot\boldsymbol{J}(\boldsymbol{r},t) \tag{2.30}$$

$$\begin{aligned}\frac{\mathrm{d}\boldsymbol{J}(\boldsymbol{r},t)}{\mathrm{d}t} =& -\iint \mathrm{d}\boldsymbol{r'}\mathrm{d}\boldsymbol{r''}\langle \boldsymbol{J}(\boldsymbol{r}),\boldsymbol{J}(\boldsymbol{r'})\rangle\cdot\nabla'\left[\langle\rho(\boldsymbol{r'})\rho(\boldsymbol{r''})\rangle^{-1}\rho(\boldsymbol{r''},t)\right] \\ & -\int_0^t \mathrm{d}t' \iint \mathrm{d}\boldsymbol{r'}\mathrm{d}\boldsymbol{r''}\boldsymbol{M}(\boldsymbol{r},\boldsymbol{r'},\boldsymbol{r''},t-t')\cdot\boldsymbol{J}(\boldsymbol{r''},t') + \mathbf{R}(\boldsymbol{r},t)\end{aligned} \tag{2.31}$$

where $\boldsymbol{M}(\boldsymbol{r},\boldsymbol{r'},\boldsymbol{r''},t) = \langle \mathbf{R}(\boldsymbol{r},t),\mathbf{R}(\boldsymbol{r'},0)\rangle\cdot\langle \boldsymbol{J}(\boldsymbol{r'}),\boldsymbol{J}(\boldsymbol{r''})\rangle^{-1}$ and $\mathbf{R}(\boldsymbol{r},t) \equiv e^{i\mathcal{Q}\mathcal{L}\mathcal{Q}t}\mathcal{Q}\dot{\boldsymbol{J}}(\boldsymbol{r})$. Equations (2.30) and (2.31) are the continuity equation and the equation of motion, respectively. These are exact equations alternative of the Liouville equations.

2.4.2 Application to attractive system

Using Eqs.(2.30) and (2.31), Yamaguchi *et al.* calculated the drag coefficient.[27] They considered that the solute is instantaneously displaced at $t = 0$ to z-direction by Δz. In the limit of small displacement Δz, the nonequilibrium average of the force from the solvent particles is represented by $\langle F_z(t)\rangle_{ne} = \xi(t)\Delta z$. Here, $\xi(t)$ is related to the drag coefficient arising from the steady solvent flow as[26]

$$\xi = \int_0^\infty \xi(t)dt. \tag{2.32}$$

When the solute-solvent interaction is represented by $u(\mathbf{r})$, the nonequilibrium average of the force is calculated by

$$\langle F_z(t)\rangle_{ne} = -\int d\mathbf{r}\frac{\partial u(\mathbf{r})}{\partial z}\bar{\rho}(\mathbf{r},t), \tag{2.33}$$

where

$$\bar{\rho}(\mathbf{r},t) = \langle\rho(\mathbf{r},t)\rangle_{ne} - \langle\rho(\mathbf{r},t=\infty)\rangle_{ne}. \tag{2.34}$$

Here, $\langle\rho(\mathbf{r},t)\rangle_{ne}$ denotes the nonequilibrium response of the solvent density around the solute. According to the linear-response theory, these nonequilibrium response is approximated by the equilibrium time correlation function as

$$\bar{\rho}(\mathbf{r},t) = \frac{1}{k_BT}\langle U(0)\rho(\mathbf{r},t)\rangle_{eq} \tag{2.35}$$

where

$$U(t) = -\int d\mathbf{r}\frac{\partial u(\mathbf{r})}{\partial z}\rho(\mathbf{r},t). \tag{2.36}$$

Since the time evolution of $\rho(\mathbf{r},t)$ is given by Eqs.(2.30) and (2.31), using Eq. (2.35) the time evolution of $\bar{\rho}(\mathbf{r},t)$ is given as

$$\frac{\mathrm{d}\bar{\rho}(\boldsymbol{r},t)}{\mathrm{d}t} = -\nabla\cdot\bar{\boldsymbol{J}}(\boldsymbol{r},t) \tag{2.37}$$

$$\begin{aligned}\frac{\mathrm{d}\bar{\boldsymbol{J}}(\boldsymbol{r},t)}{\mathrm{d}t} = &-\iint \mathrm{d}\boldsymbol{r'}\mathrm{d}\boldsymbol{r''}\langle\boldsymbol{J}(\boldsymbol{r}),\boldsymbol{J}(\boldsymbol{r'})\rangle\cdot\nabla'\left[\langle\rho(\boldsymbol{r'})\rho(\boldsymbol{r''})\rangle^{-1}\bar{\rho}(\boldsymbol{r''},t)\right]\\ &-\int_0^t \mathrm{d}t'\iint \mathrm{d}\boldsymbol{r'}\mathrm{d}\boldsymbol{r''}\boldsymbol{M}(\boldsymbol{r},\boldsymbol{r'},\boldsymbol{r''},t-t')\cdot\bar{\boldsymbol{J}}(\boldsymbol{r''},t')\end{aligned} \tag{2.38}$$

where

$$\bar{\boldsymbol{J}}(\mathbf{r},t) = \langle\boldsymbol{J}(\mathbf{r},t)\rangle_{ne} - \langle\boldsymbol{J}(\mathbf{r},t=\infty)\rangle_{ne} = \frac{1}{k_BT}\langle U(0)\boldsymbol{J}(\mathbf{r},t)\rangle_{eq}. \tag{2.39}$$

To solve Eqs. (2.37) and (2.38), they evaluated the correlation functions $\langle \boldsymbol{J}(\boldsymbol{r}), \boldsymbol{J}(\boldsymbol{r'})\rangle$, $\langle \rho(\boldsymbol{r})\rho(\boldsymbol{r'})\rangle$, and $\langle \mathbf{R}(\boldsymbol{r},t), \mathbf{R}(\boldsymbol{r'},0)\rangle$. The correlation function of the current fields is given as $\langle \boldsymbol{J}(\boldsymbol{r}), \boldsymbol{J}(\boldsymbol{r'})\rangle = k_BT/m\rho_{eq}(\boldsymbol{r})\delta(\boldsymbol{r}-\boldsymbol{r'})\mathbf{1}$ where $\mathbf{1}$ is the unit tensor. They obtained the equilibrium density field $\rho_{eq}(\boldsymbol{r})$ and the solute-solvent solvent three-body correlation function $\langle \rho(\boldsymbol{r})\rho(\boldsymbol{r'})\rangle$ using the Ornstein-Zernike integral equation coupled with the hypernetted-chain approximation (OZ/HNC theory).[46] In addition, they assumed that the time correlation function of the random force $\langle \mathbf{R}(\boldsymbol{r},t), \mathbf{R}(\boldsymbol{r'},0)\rangle$ is the same as that in the absence of the solute using the exponential model.[60], [61]

They assumed the interaction between solvent particles as the Lennard-Jones potential, where the energy and length parameters are ϵ_0 and σ, respectively. The density of the solvent waw $0.85\sigma^{-3}$ and the temperature was $0.75\epsilon_0/k_B$. They assumed the solute-solvent interaction as

$$u(r) = \begin{cases} 4\epsilon_0 \left[\left(\dfrac{\sigma}{r-(d-\sigma)/2} \right)^{12} - \left(\dfrac{\sigma}{r-(d-\sigma)/2} \right)^{6} \right] - \epsilon + \epsilon_0 \\ \qquad\qquad (r < 2^{1/6}\sigma + (d-\sigma)/2), \\ 4\epsilon \left[\left(\dfrac{\sigma}{r-(d-\sigma)/2} \right)^{12} - \left(\dfrac{\sigma}{r-(d-\sigma)/2} \right)^{6} \right] \\ \qquad\qquad (r > 2^{1/6}\sigma + (d-\sigma)/2), \end{cases} \tag{2.40}$$

where d is the diameter of the solute.

Figure 2.7 shows the calculated results of the drag coefficient as the function of the strength of solute-solvent attractive interaction. The drag coefficient increases with increasing the attractive interaction. The similar behavior has been observed in simulation studies.[29], [32], [34] When the solute is as small as the solvent, the drag coefficient deviates from the Stokes law with the attractive interaction. In contrast, when the solute is large, the drag coefficients are close to the value of the Stokes law with the stick boundary condition.

Their theory allows us to calculate the drag coefficient including the effect of the interparticle interactions. However, the calculation for the large solute is difficult because of the finite size effect in the same way as the limitation of simulations. In the case of $d = 8\sigma$, they corrected the calculated values considering the effect of the cutoff radius. To avoid the finite size effect, Inayoshi *et al.* have expanded the generalized Langevin equations with respect to the size ratio of the solute and solvent particle.[40] Using their theory, one can consider solvent particles at an infinite distance using an analytical expression of the drag coefficient. The perturbation theory will be described in Chapter 3.

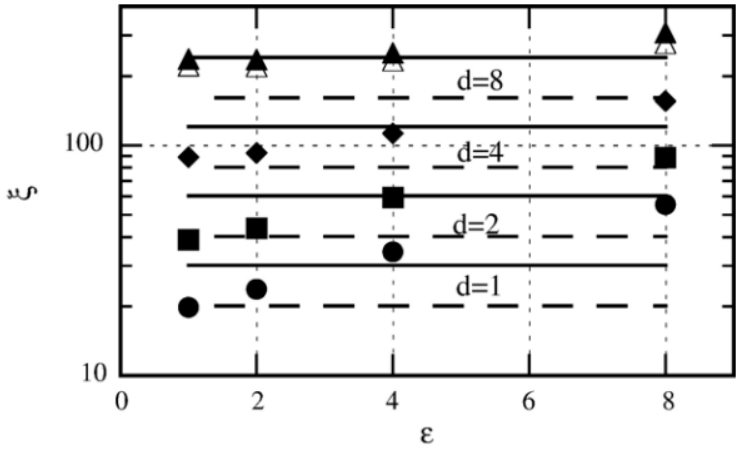

Figure 2.7 Dependence of the drag coefficient ξ on the strength of the solute-solvent attractive interaction ϵ.[27] The diameters of the solute are $d = \sigma$(circles), 2σ(squares), 4σ(diamonds), and 8σ(triangles) where σ is the diameter of the solvent particle. In Fig. 2.7, they employed the units in which the LJ parameters and mass of the solvents and the Boltzmann constant are unity. The filled symbols represent the mere values integrating $\xi(t)$, and the open symbols represent the corrected values corrected for the tail in $\xi(t)$ by the extrapolation. The solid and dashed lines represent the values predicted by the Stokes law with the slip and stick boundary conditions, respectively.

2.5 Summary

The breakdown of the Stokes law has been observed in experimental studies of a large particle diffusion.[5]–[10],[13],[14],[19],[20] As decreasing the size of the solute, the diffusion coefficient deviated from the value predicted by the SE relation.[19],[20] The deviation depended on the interparticle interaction between solute-solvent particles.[9],[10] Furthermore, the experiments for the diffusion in solvent mixtures showed the large deviations as compared to those in pure solvents.[5]–[8],[14] It was found that the diffusion coefficient has a correlation with the solvation structure around the solute.[1]–[3]

The MD simulation studies have shown that the boundary condition on the solute surface depends on the solute-solvent interaction. In the spherical interaction systems, such as the purely repulsive or weak attraction systems, the diffusion coefficient approached the SE relation with slip boundary condition when the solute becomes large.[28],[29],[31],[33],[34] In contrast, when the solute surface is rough, the diffusion

coefficient approached the SE relation with the stick boundary condition.[29],[37] In addition, some studies showed that the boundary condition changed from the slip to the stick boundary conditions with increasing the solute-solvent attractive interaction.[29],[32],[34] Although MD simulation enables us to study the interparticle interactions, the results suffer the finite-size effects.

The effects of the interparticle interactions have also been studied theoretically. Yamaguchi *et al.* formulated the generalized Langevin equations to describe the dynamics of the solvent particles around the solute.[26] Their theory is distinct from the previous theories, which do not include the effect of the solute-solvent interaction on the dynamics of the solvent particles. However, as is the case of simulation studies, the large solute cannot be treated in the theory of Yamaguchi *et al.* due to the finite-size effect. Inayoshi *et al.* avoided this difficulty, expanding the generalized Langevin equations with respect to the size ratio of the solute and solvent particle (Chap. 3).

Chapter 3

Perturbation theory

When studying a large-particle diffusion, the microscopic theories or molecular simulations suffer from the finite-size effect. To avoid this difficulty, Inayoshi *et al.* have developed a theory by perturbation expansions with respect to the size ratio of the solute and solvent particles.[40] Their theory can deal with the solvation effect through the radial distribution function, which represents the density distribution of solvent particles around the solute particle. In this chapter, I introduce the perturbation theory developed by Inayoshi *et al.* I formulate a theory on the basis of their theory in Chap. 4.

3.1 Perturbation theory

3.1.1 Basic equations

Inayoshi *et al.* assumed that solvent particles have the small velocity $\mathbf{u}$ at an infinite distance from the solute fixed to the origin to obtain the diffusion coefficient through the Einstein relation.[40] This system is equivalent to that of the solute particle moving with velocity $-\mathbf{u}$. They calculated the drag coefficient of the solute particle, by assuming the steady state. The diffusion coefficient is given by the drag coefficient through the Einstein relation (2.1).

The present system is described by the generalized Langevin equations formulated by Yamaguchi *et al.*[26] as

$$0 = -\nabla \cdot \boldsymbol{J}(\mathbf{r}), \tag{3.1}$$

$$0 = -\rho_{eq}(r)\nabla\mu(\mathbf{r}) + \int d\mathbf{r}'\mathbf{M}(\mathbf{r},\mathbf{r}')\boldsymbol{J}(\mathbf{r}'). \tag{3.2}$$

Here, $\rho_{eq}(r)$ is the equilibrium density calculated from the radial distribution function $g(r)$ through $\rho_{eq}(r) = \rho g(r)$ where ρ is the average density. At the steady state, $\mu(\mathbf{r})$ and $\boldsymbol{J}(\mathbf{r})$ can be obtained solving Eqs. (3.1) and (3.2) if $\rho_{eq}(r)$ and the memory tensor $\mathbf{M}(\mathbf{r}, \mathbf{r}')$ are given.

Since it is difficult to calculate exactly $\mathbf{M}(\mathbf{r}, \mathbf{r}')$, they employed two approximations: homogeneous approximation and long-wavelength limit approximation. Under the homogeneous assumption, $\mathbf{M}(\mathbf{r}, \mathbf{r}')$ is replaced by a homogeneous tensor which is the same as that in the absence of the solute. The same approximation was employed by Yamaguchi *et al.*[26] Additionally, they approximated the homogeneous tensor using the long-wavelength limit of the spatial Fourier transform. Thus, the second term of Eq. (3.2) is given as

$$\int d\mathbf{r}' \mathbf{M}(\mathbf{r}, \mathbf{r}') \boldsymbol{J}(\mathbf{r}') \approx \eta \nabla^2 \mathbf{v}(\mathbf{r}) + \gamma \nabla \left(\nabla \cdot \mathbf{v}(\mathbf{r}) \right). \tag{3.3}$$

Here, η is the shear viscosity, and $\gamma = \zeta + \eta/3$, where ζ is the bulk viscosity. In the absence of the solute, Equation (3.2) with the approximation (3.3) is equivalent to the average of the nonlinear fluctuation hydrodynamics.[62]–[64] It has been well studied in connection with the dynamics in supercooled liquids.

In Eq. (3.2), $\mu(\mathbf{r})$ is rewritten using the function $\mathcal{P}(\mathbf{r}) \equiv \rho_{eq}(r)\mu(\mathbf{r})$. Here, in the region far away from the solute where $\rho_{eq}(r)$ is constant, $\nabla\mathcal{P}(\mathbf{r})$ corresponds to the gradient of the pressure in the first order of the velocity $\mathbf{u}$. Owing to the symmetry of the system, $\mathbf{v}(\mathbf{r})$ and $\mathcal{P}(\mathbf{r})$ are represented as

$$\mathbf{v}(\mathbf{r}) = v_{\hat{r}}(r)(\hat{\mathbf{r}} \cdot \mathbf{u})\hat{\mathbf{r}} + v_{u,i}(r)\mathbf{u}, \tag{3.4}$$

$$\mathcal{P}(\mathbf{r}) = P(r)(\hat{\mathbf{r}} \cdot \mathbf{u}), \tag{3.5}$$

where $\hat{\mathbf{r}} = \mathbf{r}/r$.

Substituting Eqs (3.4) and (3.5) and using $\boldsymbol{J}(\mathbf{r}) = \rho_{eq}(r)\mathbf{v}(\mathbf{r})$, Eq. (3.1) is rewritten as

$$\frac{d}{dr}\left[\rho_{eq}(r) v_{\hat{r}}(r)\right] + \frac{2\rho_{eq}(r) v_{\hat{r}}(r)}{r} + \frac{d}{dr}\left[\rho_{eq}(r) v_u(r)\right] = 0, \tag{3.6}$$

and Eq. (3.2) with the approximation given by Eq. (3.3) is rewritten as

$$-\frac{P(r)}{r} + \eta\left[\frac{2v_{\hat{r}}(r)}{r^2} + \frac{2}{r}\frac{dv_u(r)}{dr} + \frac{d^2 v_u(r)}{dr^2}\right] + \gamma\left[\frac{2v_{\hat{r}}(r)}{r^2} + \frac{1}{r}\frac{dv_{\hat{r}}(r)}{dr} + \frac{1}{r}\frac{dv_u(r)}{dr}\right] = 0, \tag{3.7}$$

$$-\rho_{eq}(r)\frac{d}{dr}\frac{P(r)}{r\rho_{eq}(r)} + \eta\left[6\frac{d}{dr}\frac{v_{\hat{r}}(r)}{r^2} + r\frac{d^2}{dr^2}\frac{v_{\hat{r}}(r)}{r^2}\right] + \gamma\left[5\frac{d}{dr}\frac{v_{\hat{r}}(r)}{r^2} + r\frac{d^2}{dr^2}\frac{v_{\hat{r}}(r)}{r^2} - \frac{1}{r^2}\frac{dv_u(r)}{dr} + \frac{1}{r}\frac{d^2 v_u(r)}{dr^2}\right] = 0. \tag{3.8}$$

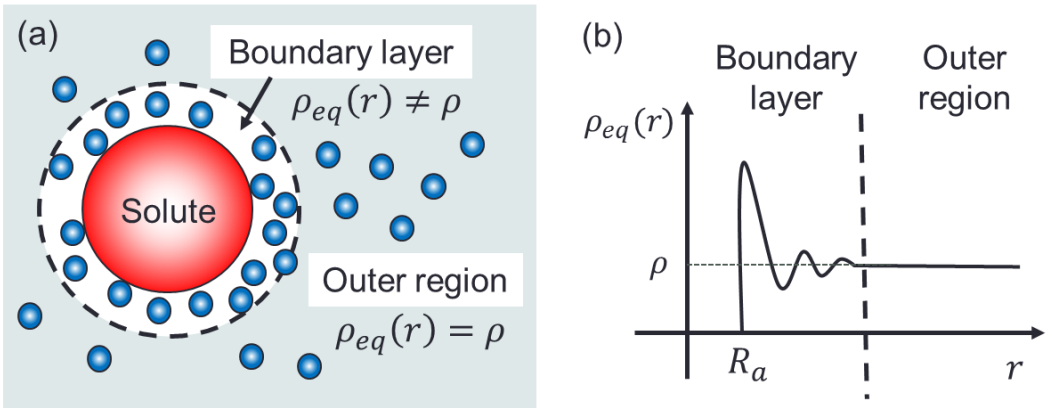

Figure 3.1 Illustration of the boundary layer and outer region: (a) The boundary layer is near the solute and the outer region is far away from the solute. The solute and solvent particles are represented as the large red and small blue spheres. (b) The equilibrium density field $\rho_{eq}(r)$. The boundary layer is defined by $\rho_{eq}(r) \neq \rho$ and the outer region is defined by $\rho_{eq}(r) = \rho$.

Equations (3.6), (3.7), and (3.8) are solved to satisfy the slip boundary condition on the solute surface as

$$\left.\frac{dv_u(r)}{dr}\right|_{r=R_a} = \frac{v_u(R_a)}{R_a}. \tag{3.9}$$

Here, $R_a = R + a$ where R and a are the radii of the solute and solvent particles, respectively. The solute surface is assumed to be at $r = R_a$ because $\rho_{eq}(r)$ vanishes for $r < R_a$.

3.1.2 Perturbation expansions

The solute particle is assumed to be much larger than the solvent particle. When the solute particle is large, it is difficult to calculate the basic equations (3.6), (3.7), and (3.8) directly because of the finite-size effect. Thus, they found approximate solutions expanding the equations in powers of the ratio between the solute and solvent size

$$\epsilon \equiv \frac{a}{R_a}. \tag{3.10}$$

They expanded the basic equations dividing the whole space into two regions depending on distance from the solute because there are two spatial scales.[65] Near the solute, the density distribution $\rho_{eq}(r)$, which is contained in the basic equations, varies in the range of solvent particle size. Thus, $v_{\hat{r}}(r)$, $v_u(r)$ and $P(r)$ also change the scale given by the solvent particle size. In contrast, in the region sufficiently far

away from the solute, the scale is given by the size of the solute because $\rho_{eq}(r)$ has constant value. The density distribution $\rho_{eq}(r)$ becomes constant at the distance of the size of several solvent particles.

Therefore, the space is divided into two regions: the outer region far away from the solute and the boundary layer near the solute (Fig. 3.1). The outer region is defined by $\rho_{eq}(r) = \rho$. The boundary layer is defined by $\rho_{eq}(r) \neq \rho$.

Since the boundary layer is dominated by the scale of the solvent particle size, they introduce a stretched variable, $x \equiv (r - R_a)/a$. Here, they assumed that $\rho_{eq}(r)$ can be represented as the function of x, $\rho_e(x)$. With the new variable x fixed, the solutions of Eqs. (3.6), (3.7), and (3.8) are expanded as

$$v_{\hat{r}}(r) = \sum_{n=0}^{\infty} \epsilon^n v_{\hat{r},b}^{(n)}(x), \tag{3.11}$$

$$v_u(r) = \sum_{n=0}^{\infty} \epsilon^n v_{u,b}^{(n)}(x), \tag{3.12}$$

$$R_a P(r) = \sum_{n=0}^{\infty} \epsilon^n P_b^{(n)}(x). \tag{3.13}$$

The left-hand side of Eq. (3.13) includes R_a so that Eqs. (3.7) and (3.8) do not explicitly have the length scale R_a or a after the substitution of Eq. (3.13) into Eqs. (3.7) and (3.8). Substituting expansion of $v_u(r)$ into Eq. (3.9), the boundary condition for the expansion coefficient of $v_{u,b}(r)$ is given by

$$\left.\frac{dv_{u,b}^{(n+1)}(x)}{dx}\right|_{x=0} = v_{u,b}^{(n)}(0). \tag{3.14}$$

In the outer region, since $\rho_{eq}(r)$ is constant, Eqs. (3.1) and (3.2) with Eq. (3.3) reduced to the incompressible hydrodynamic equations as

$$\nabla \cdot \mathbf{v}(\mathbf{r}) = 0, \tag{3.15}$$

$$-\nabla \mathcal{P}(\mathbf{r}) + \eta \nabla^2 \mathbf{v}(\mathbf{r}) = 0. \tag{3.16}$$

Unlike the boundary layer, they defined a variable as $\bar{r} \equiv r/R_a$ since the outer region is dominated by the scale of the solute particle size. Thus, in the outer region, the

solutions are expanded as

$$v_{\hat{r}}(r) = \sum_{n=0}^{\infty} \epsilon^n v_{\hat{r},o}^{(n)}(\bar{r}), \tag{3.17}$$

$$v_u(r) = \sum_{n=0}^{\infty} \epsilon^n v_{u,o}^{(n)}(\bar{r}), \tag{3.18}$$

$$R_a P(r) = \sum_{n=0}^{\infty} \epsilon^n P_o^{(n)}(\bar{r}). \tag{3.19}$$

with $\bar{r} \equiv r/R_a$ fixed. The left-hand side of Eq. (3.19) includes R_a for the same reason as for Eq. (3.13).

Connecting condition

They assumed that the boundary layer solutions are required to be consistent with the outer solutions at $x \to \infty$ as

$$\lim_{x\to\infty} \{X_b(x) - X_o(\bar{r})\} = 0. \tag{3.20}$$

Here, $X_b(x)$ and $X_o(\bar{r})$ are any of $v_{\hat{r}}(r)$, $v_u(r)$, and $P(r)$ in the boundary layer and outer region. Since $\bar{r} = 1 + \epsilon x$, the expansion of $X_o(\bar{r})$ around $\bar{r} = 1$ gives

$$\lim_{x\to\infty} \left\{ X_b(x) - \sum_{n=0}^{\infty} \frac{\epsilon^n x^n}{n!} \frac{d^n X_o(\bar{r})}{d\bar{r}^n}\bigg|_{\bar{r}=1} \right\} = 0. \tag{3.21}$$

Substituting the expansions of $X_b(x)$ and $X_o(\bar{r})$, such as Eqs. (3.11) and (3.17), into Eq. (3.21), the connecting condition between the solutions is obtained as

$$C_m^{(n)} = \frac{1}{m!} \frac{d^m X_o^{(n-m)}(\bar{r})}{d\bar{r}^m}\bigg|_{\bar{r}=1}. \tag{3.22}$$

Here, $C_m^{(n)}$ is constant defined by an asymptotic form of boundary layer solution

$$X_{bl}^{(n)}(x) \xrightarrow[x\to\infty]{} \sum_{m=0}^{\infty} C_m^{(n)} x^m, \tag{3.23}$$

where

$$C_m^{(n)} = 0 \; for \; n - m > 0. \tag{3.24}$$

3.1.3 Boundary conditions for the outer region

Equation (3.22) shows that the boundary layer solutions give the boundary conditions of the outer solutions at $\bar{r} = 1$. Inayoshi *et al.* derived the boundary condition of outer solutions by Eq. (3.22) and solved the outer equations (3.15) and (3.16). From the outer solution of $\mathbf{v}(\mathbf{r})$ and $\mathcal{P}(\mathbf{r})$, they obtained the drag coefficient.

The boundary conditions of the outer region are derived as follows. First, substituting $r = R_a + ax$ and the expansions of $v_{\hat{r}}(r)$, $v_u(r)$, and $P(r)$ for the boundary layer, Eqs. (3.6) - (3.8) are expanded in a power series of ϵ. Then, these differential equations are solved under the slip boundary condition given by Eq. (3.14). Finally, using the boundary layer solutions and Eq. (3.22), the boundary conditions of the outer solution are obtained. Details of the derivation are given in Chap. 5.

They derived the boundary conditions proportional to ϵ^0 as

$$v^{(0)}_{\hat{r},o}(1) + v^{(0)}_{u,o}(1) = 0, \tag{3.25}$$

$$\left.\frac{dv^{(0)}_{u,o}(\bar{r})}{d\bar{r}}\right|_{\bar{r}=1} = v^{(0)}_{u,o}(1). \tag{3.26}$$

Equation (3.26) is in agreement with the slip boundary condition given by Eq. (3.14).

The boundary conditions proportional to ϵ^1 are derived as

$$v^{(1)}_{\hat{r},o}(1) + v^{(1)}_{u,o}(1) = \alpha v^{(0)}_{u,o}(1), \tag{3.27}$$

$$\left.\frac{dv^{(1)}_{u,o}(\bar{r})}{d\bar{r}}\right|_{\bar{r}=1} - v^{(1)}_{u,o}(1) = \frac{\alpha}{2\eta}P^{(0)}_o(1) - \beta v^{(0)}_{u,o}(1). \tag{3.28}$$

Here, α and β are given as

$$\epsilon\alpha = \frac{2}{R+a}\int_{R+a}^{\infty}\left[\frac{\rho_{eq}(r)}{\rho_{eq}(\infty)} - 1\right]dr, \tag{3.29}$$

$$\epsilon\beta = \frac{1}{R+a}\left\{\int_{R+a}^{\infty}\Delta v(r)dr - \left(1+\frac{\gamma}{\eta}\right)\left[\int_{R+a}^{\infty}\rho_{eq}(r)\int_{r}^{\infty}\frac{\omega(r')}{\rho_{eq}(r')}\Delta v(r')dr'dr\right\}\right. \tag{3.30}$$

where

$$\Delta v(r) = \frac{2\omega(r)}{\rho_{eq}(r)}\int_{R+a}^{r}\rho_{eq}(r')dr', \tag{3.31}$$

$$\omega(r) = \frac{1}{\rho_{eq}(r)}\frac{d\rho_{eq}(r)}{dr}. \tag{3.32}$$

The first-order boundary conditions are determined by $\rho_{eq}(r)$ through the parameters α and β in contrast to the zeroth-order boundary conditions.

3.1.4 Drag coefficient

The outer equations (3.15) and (3.16) are solved analytically under the condition of $\mathbf{v}(\mathbf{r}) = \mathbf{u}$ at $r \to \infty$. The solutions proportional to ϵ^0 are represented as

$$v_{\hat{r}}(r) = -\frac{c^{(0)} R_a}{8r} + \frac{3d^{(0)} R_a^3}{r^3}, \tag{3.33}$$

$$v_u(r) = 1 - \frac{c^{(0)} R_a}{8r} - \frac{d^{(0)} R_a^3}{r^3}, \tag{3.34}$$

$$P_s(r) = -\frac{c^{(0)} R_a}{4r^2}\eta. \tag{3.35}$$

Since these solutions satisfy the boundary conditions Eqs. (3.25) and (3.26), the constants $c^{(0)}$ and $d^{(0)}$ are derived as

$$c^{(0)} = 4, \tag{3.36}$$

$$d^{(0)} = 0. \tag{3.37}$$

The solutions proportional to ϵ^1 are represented as

$$v_{\hat{r}}(r) = -\frac{c^{(1)} R_a}{8r} + \frac{3d^{(1)} R_a^3}{r^3}, \tag{3.38}$$

$$v_u(r) = -\frac{c^{(1)} R_a}{8r} - \frac{d^{(1)} R_a^3}{r^3}, \tag{3.39}$$

$$P_s(r) = -\frac{c^{(1)} R_a}{4r^2}\eta. \tag{3.40}$$

In the same way as for zeroth-order solutions, using the boundary conditions Eqs. (3.27) and (3.28), the constants $c^{(1)}$ and $d^{(1)}$ are obtained as

$$c^{(1)} = -2\alpha - \frac{2\beta}{3}, \tag{3.41}$$

$$d^{(1)} = -\frac{\beta}{12}. \tag{3.42}$$

where α and β are given by Eqs. (3.29) and (3.30).

From these solutions, the drag coefficient ξ is derived as

$$\xi = c\pi\eta R_a, \tag{3.43}$$

$$c = c^{(0)} + \epsilon c^{(1)} = 4 - 2\epsilon\alpha - \frac{2\epsilon\beta}{3}. \tag{3.44}$$

The terms higher than the second order of ϵ are omitted. The diffusion coefficient is obtained from the drag coefficient through the Einstein relation.

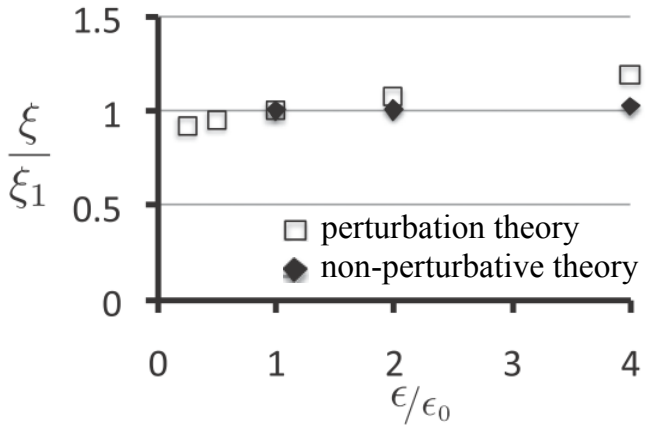

Figure 3.2 The ratio of the drag coefficients ξ/ξ_1 as a function of the strength of the attraction between solute and solvent particles ϵ in Eq. (3.45).[40] Here, ξ_1 is the value when $\epsilon = \epsilon_0$ where ϵ_0 is the energy parameters of the interaction between solvent particles given by the Lennard-Jones potential. Open symbols represent the results of the perturbation theory and filled symbols represent the results of the non-perturbative theory derived by Yamaguchi *et al.*[27] The diameter of the solute sphere is $d = 8\sigma$ where σ is the diameter of the solvent spheres. Note that I added the description of symbols to the original figure.

Equation (3.43) depends on the solvation structure because α and β include $\rho_{eq}(r)$ as shown by Eqs (3.29) and (3.30). When the solvation structure is inhomogeneous, that is, $\rho_{eq}(r) \neq \rho$, α and β are not zero. In this case, the drag coefficient deviates from the Stokes law with the slip condition.

3.2 Application to Kihara potential system

Inayoshi *et al.* have applied their theory to the attractive interaction system. The solute-solvent interaction is given by Kihara potential as

$$u(r) = 4\epsilon \left[\left(\frac{\sigma}{r - (d-\sigma)/2} \right)^{12} - \left(\frac{\sigma}{r - (d-\sigma)/2} \right)^{6} \right], \tag{3.45}$$

where d and σ are the diameters of the solute and solvent particles, respectively. The parameter ϵ represents the strength of the attractive force. The interaction between solvent particles is given by the Lennard-Jones potential, where the energy and length parameters are ϵ_0 and σ, respectively. They assumed $d = 8\sigma$, the solvent

density of $0.85\sigma^{-3}$, and the temperature of $0.75\epsilon_0/k_B$. Additionally, they assumed $\gamma = 0$ in Eq. (3.30).

The calculated results were compared with those calculated by Yamaguchi *et al.* using the non-perturbative theory. Yamaguchi *et al.* calculated the drag coefficient for the similar potential system given by Eq. (2.40). Equation (2.40) reduces to Eq. (3.45) when $\epsilon = \epsilon_0$. By comparing results calculated by two theories, Inayoshi *et al.* discussed the the validity of the approximation of Memory tensor and the perturbation expansion.

Inayoshi *et al.* showed that ϵ-dependence of the drag coefficient is qualitatively in agreement with that given by the non-perturbative theory. Figure 3.2 shows the ratio ξ/ξ_1, where ξ_1 is the value when $\epsilon = \epsilon_0$. The difference between the two theories is less than 17% in the range $\epsilon < 4\epsilon_0$. However, the absolute values of ξ is about 1.5 times larger than those of the non-perturbative theory. They considered that this deviation decreases with increasing the solute diameter.

3.3 Summary

Inayoshi *et al.* have formulated a perturbation theory to study the solvation effects on a large-particle diffusion.[40] They expanded the generalized Langevin equations in powers of the size ratio of the solute and solvent particles. The expansion allows one to derive hydrodynamic equations with boundary conditions which depend on the density distribution of solvent particles. Solving these equations, they obtained an analytical expression of the drag coefficient of a large solute.

The perturbation theory has two merits comparing with the previous theories. The first is that one can consider the solvation effects on the diffusion through the radial distribution function, which can be derived by MD simulations or the integral equations for liquids. The solvation effects are not considered in the Stokes-Einstein relation. The second is that the theory does not suffer the finite-size effect. One can consider solvent particles at an infinite distance using an analytical solutions of hydrodynamic equations. Thus, one can treat larger solute particle than the solvent particle.

Inayoshi *et al.* showed that the drag coefficient calculated by the perturbation theory is 1.5 times larger than that obtained by the non-perturbative theory in the attractive interaction system.[27] In order to quantitatively evaluate the drag coefficient, the improvement is required in the perturbation theory.

Chapter 4

Study for one-component solvent system

Inayoshi *et al.* have formulated the perturbation theory to study the solvation effects on the diffusion.[40] However, their theory gives the drag coefficient much larger than that calculated by the non-perturbative theory. In the present chapter, I formulate a new perturbation theory on the basis of the theory developed by Inayoshi *et al.* Furthermore, I show that the results calculated by the present theory are in good agreement with those of the non-perturbative theory and MD simulations.

4.1 New expression of drag coefficient

Inayoshi *et al.* derived the hydrodynamic equations and the boundary conditions on the solute surface up to the first order of ϵ by perturbation expansions. Under the derived boundary conditions, they solved the hydrodynamic equations by omitting terms higher than the first order of ϵ. In the present study, in contrast to the theory of Inayoshi *et al.*, I consider higher terms of the hydrodynamic equations when solving these equations with the derived boundary conditions.

From Eqs. (3.25)-(3.28), by omitting terms higher than the first order of ϵ, the boundary conditions are rewritten as follows:

$$v_{\hat{r}}(R_a) + v_u(R_a) = \epsilon\alpha v_u(R_a), \tag{4.1}$$

$$\left.\frac{dv_u(r)}{dr}\right|_{r=R_a} = \frac{1-\epsilon\beta}{R_a} v_u(R_a) + \frac{\epsilon\alpha}{2\eta} P_s(R_a). \tag{4.2}$$

The parameters α and β are given by Eqs (3.29) and (3.30), respectively.

The solutions of the hydrodynamic equations (3.15) and (3.16) are obtained as

$$v_{\hat{r}}(r) = -\frac{cR_a}{8r} + \frac{3dR_a^3}{r^3}, \tag{4.3}$$

$$v_u(r) = 1 - \frac{cR_a}{8r} - \frac{dR_a^3}{r^3}, \tag{4.4}$$

$$P_s(r) = -\frac{cR_a}{4r^2}\eta. \tag{4.5}$$

under the condition of $\mathbf{v}(\mathbf{r}) = \mathbf{u}$ at $r \to \infty$. To satisfy Eqs. (4.1) and (4.2), the constants c and d are determined as

$$c = \frac{48 - 24\epsilon\alpha - 24\epsilon\beta}{12 - 4\epsilon\beta + (\epsilon\alpha)^2}, \tag{4.6}$$

$$d = \frac{-\epsilon\beta + (\epsilon\alpha)^2}{12 - 4\epsilon\beta + (\epsilon\alpha)^2}. \tag{4.7}$$

From Eqs. (4.3) - (4.5), the drag coefficient ξ is derived as

$$\xi = c\pi\eta R_a, \tag{4.8}$$

where c is given by Eq. (4.6).

Equation (4.6) is different from Eq. (3.44) derived by Inayoshi *et al.* Equation (4.6) includes nonlinear terms of ϵ. It is reduced to Eq. (3.44) when Eq. (4.6) is linearized for ϵ.

4.2 Validity of the theory

I have obtained the new expression of c including nonlinear terms of ϵ. To confirm the validity of the present theory, I compare the calculated results with those obtained using the non-perturbative theory and MD simulations.

4.2.1 Comparison with previous perturbation theory

In this subsection, I calculate c using the new expression of c given by Eq. (4.6). The calculated results are compared with those obtained using the previous expression of c derived by Inayoshi *et al.*, that is, Eq. (3.44). In both expressions, c depends on the parameter α and β, which are given by Eqs (3.29) and (3.30), respectively. Equations (3.29) and (3.30) are calculated from the radial distribution function between the solute and solvent particles, $g(r)$. Although $g(r)$ should be determined

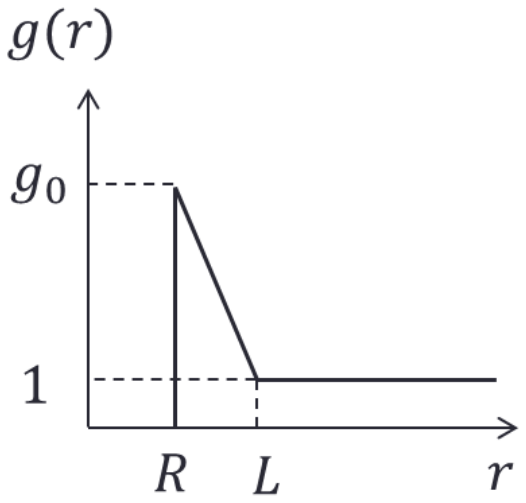

Figure 4.1 Model radial distribution function given by Eq. (4.9).

by the interparticle interactions, I assume a simple model of $g(r)$ in this study as

$$g(r) = \begin{cases} -\dfrac{g_0 - 1}{L - R}(r - L) + 1 & R \leq r < L, \\ 1 & L \geq r \end{cases} \tag{4.9}$$

where g_0 and $L = R + a$ represent the peak and width of $g(r)$, respectively. Figure 4.1 shows $g(r)$ given by Eq. (4.9).

Substituting Eq. (4.9) into Eqs (3.29) and (3.30), α and β are calculated analytically as[40]

$$\alpha = g_0 - 1, \tag{4.10}$$

$$\beta = -\frac{(1 + \gamma/\eta)}{6}(g_0 - 1)^2(g_0 + 3) + (1 - g_0). \tag{4.11}$$

I assume for simplicity that the bulk viscotiy is zero, that is, $\gamma = \eta/3$. In addition, the radius of the solute particle is $R = 10a$ where a is the radius of the solvent particle.

Figure 4.2 shows the dependence of c on the peak value of $g(r)$, g_0. When $g_0 < 5$, the results calculated using the present theory are in good agreement with those of Inayoshi *et al.* However, the results of the present theory deviate from those of Inayoshi *et al.* when $g_0 > 5$. While the results of the present theory approach $c = 6$ (the stick boundary condition), the results of Inayoshi increase rapidly with increasing g_0.

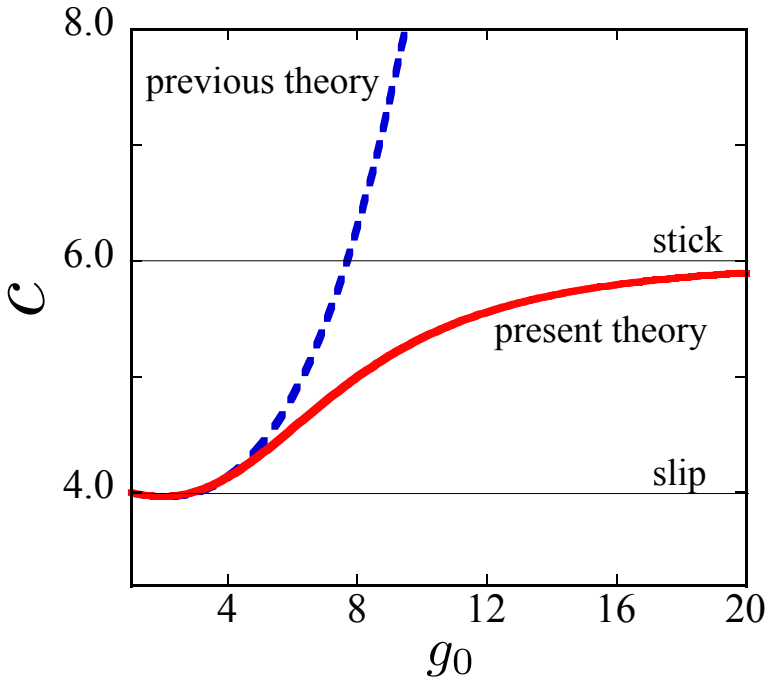

Figure 4.2 Dependence of the boundary condition coefficient c on the peak value of $g(r)$, g_0, where $g(r)$ is given by Eq. (4.9). Solid and dashed curves represent the results calculated using the present theory given by Eq. (4.6) and the previous theory of Inayoshi *et al.* given by Eq. (3.44), respectively. Solid lines at $c = 4$ and 6 denote slip and stick boundary conditions, respectively. In Eq. (4.9), $R = 10a$ and $L = 11a$ where a is the radius of the solvent particle.

Large value of c gives the large drag coefficient through Eq. (4.8). Thus, according to the results of Inasyoshi *et al.*, the drag coefficient diverges when g_0 has an infinite value. The large value of g_0 represents that solvent particles accumulate around the solute particle. It is not expected that a layer of solvent particles on the solute surface causes the infinite value of the drag coefficient. I consider that the results of Inayoshi *et al.* overestimate the solvation effects.

The results of the new theory avoid divergence of the drag coefficient. This results can also be explained by the new expression of c given by Eq. (4.6). One finds that from Eqs. (4.10) and (4.11), α and β are proportional to g_0 and g_0^3 in the large g_0 limit, respectively. Thus, β diverges faster than α at $g_0 \to \infty$. It causes $c \to 6$. In contrast, when c is given by Eq. (3.44), $c \to \infty$ at $g_0 \to \infty$. While c given by Eq. (3.44) is the linearized expression for ϵ, the new expression c given by Eq. (4.6) includes nonlinear terms of ϵ. I can consider that the present theory gives reasonable value even when g_0 has a large value.

4.2.2 Comparison with non-perturbative theory

In this subsection, I compare the calculated results with those obtained using the non-perturbative theory formulated by Yamaguchi *et al.*[26],[27] As shown in Chap. 2.4, they obtained the drag coefficient by solving the generalized Langevin equations (2.37) and (2.38) numerically without perturbation expansions. Their equations are employed as the basic equations in the present theory.

The system is the same as that in Chap. 2.4.2. The interaction between solvent particles is given the Lennard-Jones potential. The solute-solvent interaction is given by Eq. (2.40). The density of the solvent is $0.85\sigma^{-3}$ and the temperature is $0.75\epsilon_0/k_B$. The radial distribution functions $g(r)$ of the above system are obtained using the Ornstein-Zernike integral equation coupled with the hypernetted-chain closure (OZ/HNC theory).[46]

To calculate the drag coefficient, one needs to evaluate the values of γ/η included in Eq. (3.30) and η included in Eq. (4.8). I obtain the value of the shear viscosity η from the MD simulation by Yamaguchi *et al.*[36] In addition, I assume that the bulk viscosity is zero, that is, $\gamma = \eta/3$ in Eq. (3.30). The drag coefficient does not change greatly by the bulk viscosity. I have found that the difference between the drag coefficients at $\gamma = \eta/3$ and $\gamma = 0$ is less than 2%.

The results of the present perturbation theory are in good agreement with those of the non-perturbative theory when the solute particle is large. Figure 4.3 shows the ϵ-dependence of the dimensionless drag coefficient $\xi^* \equiv \xi(\sigma^2/\epsilon_0 m)^{1/2}$, where m is the mass of the solvent particle. When the solute sphere is small, the results of the present theory are significantly different from those of the non-perturbative theory Although the drag coefficient of the non-perturbative theory increases with ϵ, those of the present theory change hardly. However, when the solute sphere becomes larger, ϵ-dependence of the present theory approaches to that of the non-perturbative theory.

In Fig. 4.4, I plot the difference between the drag coefficients obtained by the present perturbation theory and non-perturbative theory, $\Delta\xi \equiv (\xi_p - \xi_n)/\xi_n$ as a function of the diameter of the solute sphere. When $d = \sigma$, the results obtained by the present theory deviate significantly from those obtained from the non-perturbative theory. For instance, the deviation is 46% at $\epsilon = 8\epsilon_0$ when $d = \sigma$. However, the deviation from the results of the non-perturbative theory decreases with increasing solute particle size. When $d = 8\sigma$, the deviation is less than 14% at $\epsilon = 8\epsilon_0$.

Since the present theory is an approximation of the non-perturbative theory, the results of the non-perturbative theory are more accurate than those of the present

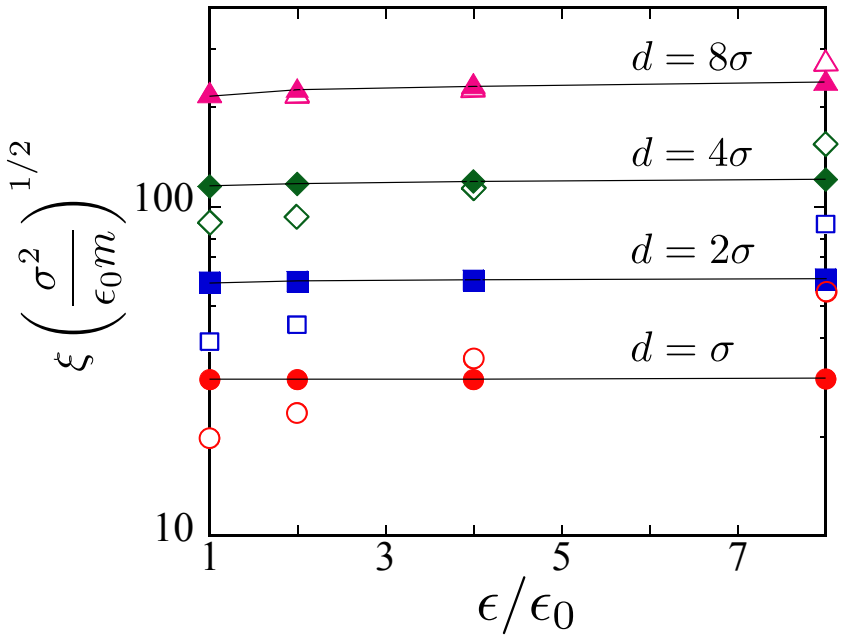

Figure 4.3 The drag coefficient ξ as a function of the strength of the attraction between solute and solvent particles ϵ in Eq. (2.40). The interaction between solvent particles is given by the Lennard-Jones potential, where the energy and length parameters are ϵ_0 and σ, respectively. Filled symbols represent the results obtained by the present perturbation theory and open symbols represent the results of the non-perturbative theory calculated by Yamaguchi *et al.*[27] The diameters of the solute spheres d are σ (circles), 2σ (squares), 4σ (diamonds), and 8σ (triangles). The solid lines are drawn to guide the eye.

theory. As shown above, the results of the present theory deviate from those of the non-perturbative theory for the small solutes while the deviation decreases with increasing the solute size. I can consider that the large deviation for the small solutes is caused by the perturbation expansion with respect to the size ratio between the solute and solvent particles. Our approximation becomes more reasonable as the solute size increases. Thus, it is expected that the difference in the results for the two theories will become smaller as the solute size increases.

4.2.3 Comparison with molecular dynamics simulation

In this subsection, I compare the calculated results for hard-sphere systems with those obtained by MD simulations. I employ the data of the MD simulations calculated by Sokolovskii *et al.*[28] as shown in Chap. 2.3.1. The systems are composed of

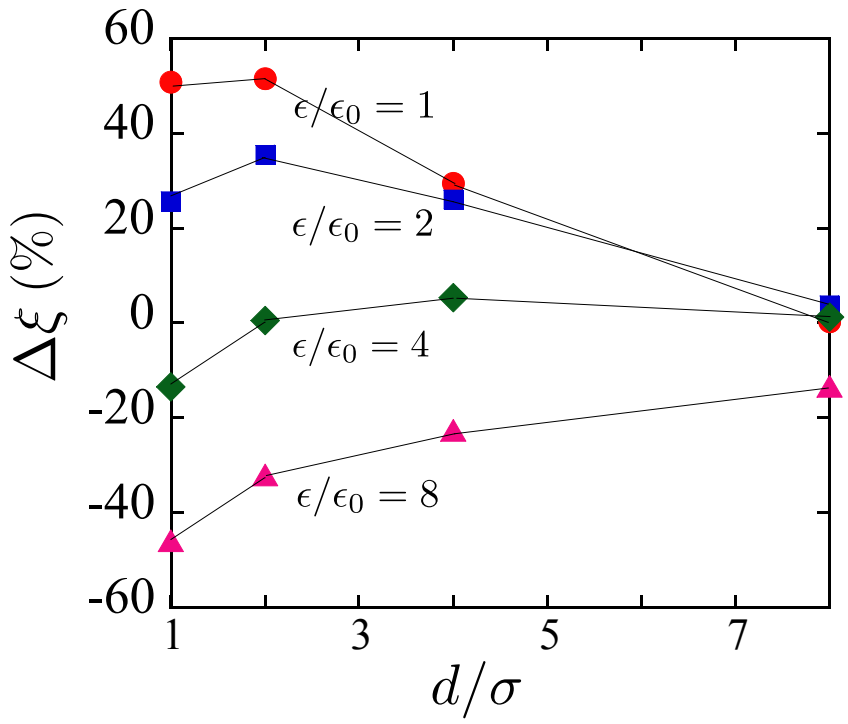

Figure 4.4 The difference between the drag coefficients obtained by the present perturbation theory ξ_p and non-perturbative theory ξ_n. Here, $\Delta\xi \equiv (\xi_p - \xi_n)/\xi_n$. The strength of the attraction between solute and solvent particles ϵ are ϵ_0 (circles), $2\epsilon_0$(squares), $4a$ (diamonds), and $8a$ (upward triangles) The solid lines are drawn to guide the eye.

a hard-sphere solute and a one-component hard-sphere solvent. The packing fraction of the solvent is 0.27. The radius of the solute sphere R increases from a to $17a$, where a is the radius of a solvent sphere.

I obtain the radial distribution function $g(r)$ of the hard-sphere system using OZ/HNC theory. For the numerical calculation, a hybrid convergence algorithm is employed.[66]–[71] In addition, I assume $\gamma = \eta/3$. The shear viscosity η is evaluated from the diffusion coefficient obtained from the SE relation, which is calculated by Sokolovskii *et al.*

Figure 4.5 shows the reduced diffusion coefficient $D^* \equiv D(mR_a^2/\sigma^4 k_B T)^{1/2}$, where $R_a = R + a$, $\sigma = 2a$, and m is the mass of the solvent sphere. The reduced diffusion coefficient calculated by the SE relation is constant regardless of the size ratio R_a/σ. The results of the present perturbation theory are in agreement with those of the MD simulations when the solute radius is larger than $7a$ ($R_a/\sigma = 4$). The results of the present theory are close to the values obtained from the SE relation with the slip

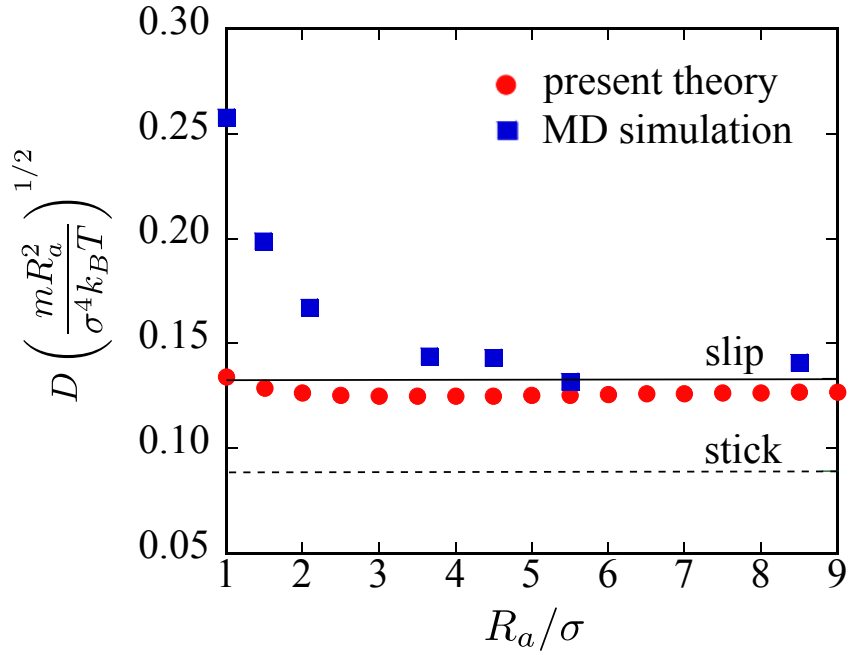

Figure 4.5 Diffusion coefficient D of a hard-sphere system as a function of the solute sphere radius R. Here, $R_a = R + a$ and $\sigma = 2a$ where R and a are the radii of the solute and solvent spheres, respectively. Filled circles represent results obtained by the present perturbation theory and filled squares represent the results of MD simulations calculated by Sokolovskii *et al.*[28] The solid and dashed lines show the Stokes-Einstein relation with slip and stick boundary conditions, respectively. The packing fraction of the solvent is 0.27.

boundary condition regardless of the solute size. In contrast, the results of the MD simulations have larger values than those of the slip boundary condition for small solutes, However, they approach the value of the slip condition with increasing the solute radius. The result obtained by the new theory is 5% smaller than that of the MD simulations when $R = 10a$ ($R_a/\sigma = 5.5$).

The large deviations from the slip boundary condition for the small solutes have also been observed in other MD simulations.[29], [31], [33] This behavior indicates the breakdown of hydrodynamics for the small solutes.[31] In contrast, the large deviation is not observed in the results of the present perturbation theory. This is because the present perturbation theory is formulated assuming that the solute particle is much larger than the solvent particle. The present theory is not appropriate to study of the small solutes for which the diffusion coefficient deviates from the SE relation significantly.

4.3 Summary

I have extended the perturbation theory developed by Inayoshi *et al.* While Inayoshi *et al.* solved the hydrodynamic equations by omitting terms higher than the first order of ϵ, I solve them by taking into account the higher terms of ϵ. I derived a new expression of c which includes nonlinear terms of ϵ. Using the present theory, I calculated c of the simple model of the radial distribution function. The results showed that the present theory can avoid the divergence of c when the solvent density is high around the solute particle in contrast to the theory of Inayoshi *et al.*

I also compared the calculated results with those obtained by the non-perturbative theory[26],[27] and MD simulation.[28] The comparison showed that the present theory becomes more accurate as the size ratio increases. The calculation results were in good agreement with those of other theories when the size ratio between the solute and solvent particles is larger than 7. This is because the present theory is formulated on the basis of the perturbation expansion with respect to the size ratio of the solute and solvent particles.

Chapter 5

Perturbation theory for two-component solvent mixture

When a solvent consists of more than one components, the solvation structure can greatly affect the diffusion coefficient. For instance, the density of a binary solvent around a solute particle is much higher than the bulk density due to the excluded volume effect.[72] In fact, some experiments on mixtures have shown the breakdown of the Stokes law.[5]–[8],[13],[14] The solvation effect on the diffusion in multi-component solvent systems, however, has not been well understood theoretically.

In this chapter, in order to study the solvation effect, I formulate a theory of the drag coefficient of a large spherical particle in a binary solvent.[73]–[75] The drag coefficient in a multi-component solvent system cannot be studied by the perturbation theory in Chap. IV. Thus, to treat a binary solvent system, I employ the generalized Langevin equations for a two-component inhomogeneous fluid as the basic equation. These equations are expanded using singular perturbation techniques similar to the one-component case.[40]

5.1 Basic equations

I consider the system where a large solute particle is immersed in a binary mixture consisting of particles of solvents 1 and 2. The solvent particles have the small velocity $\mathbf{u}$ at an infinite distance from the solute fixed to the origin. The particle radii of solute, solvent 1, and solvent 2 are denoted by R, a, and b, respectively. The solvents 1 and 2 are assumed to be much smaller than the size of the solute particle ($a, b \ll R$). Additionally, the particles of solvent 2 are greater than or equal to the particles of solvent 1 ($a \leq b$). All particles are electrically neutral and interact with

spherically symmetric potentials.

5.1.1 Generalized Langevin equations for two-component solvent system

As is the case of a one-component solvent system,[26],[40] the dynamics of solvent particles around the solute is given by the generalized Langevin equations using the projection operator method.[26] I project all phase functions, time developments of the mass-density and the current-density fields of each solvent species, into the subspace of these fields. The nonequilibrium ensemble averages of the mass-density and the current-density fields of solvent i around the solute are denoted by $\langle w_i(\mathbf{r},t)\rangle_{ne}$ and $\langle \mathbf{J}_i(\mathbf{r},t)\rangle_{ne}$, respectively.

The time developments of $w_i(\mathbf{r},t) \equiv \langle w_i(\mathbf{r},t)\rangle_{ne} - \langle w_i(\mathbf{r},t=\infty)\rangle_{ne}$ and $\mathbf{J}_i(\mathbf{r},t) \equiv \langle \mathbf{J}_i(\mathbf{r},t)\rangle_{ne} - \langle \mathbf{J}_i(\mathbf{r},t=\infty)\rangle_{ne}$ are given as

$$\frac{\partial w_i(\mathbf{r},t)}{\partial t} = -\nabla\cdot\boldsymbol{J}_i(\mathbf{r},t), \tag{5.1}$$

$$\frac{\partial \boldsymbol{J}_i(\mathbf{r},t)}{\partial t} = -w_{i,eq}(r)\nabla\mu_i(\mathbf{r},t) + \int_0^t dt' \int d\mathbf{r}' \sum_{j=2}^{2} \mathbf{M}_{ij}(\mathbf{r},\mathbf{r}',t-t')\boldsymbol{J}_i(\mathbf{r}',t), \tag{5.2}$$

where the function $\mu_i(\mathbf{r},t)$ of the first term on the right hand side of Eq. (5.2) is defined in terms of the density correlation function of the solvent.[26] The function $\mathbf{M}_{ij}(t-t',\mathbf{r},\mathbf{r}')$ of the second term denotes the memory tensor. Here, $w_{i,eq}(r)$ is the equilibrium mass-density field of solvent i in a binary solvent mixture when $\mathbf{u}=0$. The equilibrium mass-density field of solvent i depends only on the distance from the solute r. When r is sufficiently large, $w_{i,eq}(r)=\rho_i$ where ρ_i is the bulk mass density of solvent i. In the region where $w_{1,eq}(r)=\rho_1$ and $w_{2,eq}(r)=\rho_2$, $\Sigma_i w_{i,eq}(r)\nabla\mu_i(\mathbf{r},t)$ corresponds to the gradient of the pressure in the first order of the velocity $\mathbf{u}$.

5.1.2 Approximation of memory terms

I approximate the memory tensor $\mathbf{M}_{ij}(t-t',\mathbf{r},\mathbf{r}')$ in the long-wave limit given using the compressible hydrodynamics for a two-component inhomogeneous fluid. According to the hydrodynamics for a two-component fluid,[76],[77] the equations of motion are described in terms of the barycentric flow (total momentum) $\boldsymbol{J}(\mathbf{r},t)$ and

diffusional flow $\boldsymbol{J}_d(\mathbf{r},t)$ defined as

$$\boldsymbol{J}(\mathbf{r},t) \equiv w_T(\mathbf{r},t)\mathbf{v}(\mathbf{r},t), \tag{5.3}$$

$$\begin{aligned}\boldsymbol{J}_d(\mathbf{r},t) &\equiv w_1(\mathbf{r},t)\left[\mathbf{v}_1(\mathbf{r},t)-\mathbf{v}(\mathbf{r},t)\right] \\ &= -w_2(\mathbf{r},t)\left[\mathbf{v}_2(\mathbf{r},t)-\mathbf{v}(\mathbf{r},t)\right].\end{aligned} \tag{5.4}$$

Here, $w_T(\mathbf{r},t) = w_1(\mathbf{r},t) + w_2(\mathbf{r},t)$ and $\mathbf{v}(\mathbf{r},t) = \sum_i w_i(\mathbf{r},t)\mathbf{v}_i(\mathbf{r},t)/w_T(\mathbf{r},t)$, which is called the barycentric velocity.

According to the hydrodynamics for a two-component fluid, the time development of $\boldsymbol{J}(\mathbf{r},t)$ and $\boldsymbol{J}_d(\mathbf{r},t)$ are given as follows:[76],[77]

$$\frac{\partial \boldsymbol{J}(\mathbf{r},t)}{\partial t} = -\nabla P(\mathbf{r},t) + \eta\nabla^2\mathbf{v}(\mathbf{r},t) + \gamma\nabla\left[\nabla\cdot\mathbf{v}(\mathbf{r},t)\right] - \sum_i^2 w_i(\mathbf{r},t)\nabla\phi_i(r)/m_i, \tag{5.5}$$

$$\begin{aligned}\frac{\partial \boldsymbol{J}_d(\mathbf{r},t)}{\partial t} =& w_1(\mathbf{r},t)\left[\nabla\mu_1(\mathbf{r},t) - \sum_i^2 w_i(\mathbf{r},t)\nabla\mu_i(\mathbf{r},t)/w_T(\mathbf{r},t)\right] \\ &- L\left[\mathbf{v}_1(\mathbf{r},t)-\mathbf{v}_2(\mathbf{r},t)\right].\end{aligned} \tag{5.6}$$

In Eq. (5.5), $P(\mathbf{r},t)$ is the pressure, η is the shear viscosity of a binary solvent, and $\gamma = \zeta + \eta/3$, where ζ is the bulk viscosity. In the forth term on the right hand side of Eq. (5.5), m_i is the mass of particles of solvent i and $\phi_i(r)$ is the external field imposed on the fluid i. The external field represents the interaction potential between the solute and solvent particle i, where r is the distance from the solute. In Eq. (5.6), $\mu_i(\mathbf{r},t)$ is the chemical potential of solvent i, and L represents the strength of the friction between solvents 1 and 2.

Using the definitions in Eqs. (5.3) and (5.4), from Eqs. (5.5) and (5.6), the time development for $w_i(\mathbf{r},t)\mathbf{v}_i(\mathbf{r},t)$ is derived as

$$\begin{aligned}\frac{\partial w_i(\mathbf{r},t)\mathbf{v}_i(\mathbf{r},t)}{\partial t} =& \frac{w_{i,eq}(r)}{w_{T,eq}(r)}\frac{\partial \boldsymbol{J}(\mathbf{r},t)}{\partial t} \pm \frac{\partial \boldsymbol{J}_d(\mathbf{r},t)}{\partial t} \\ =& -w_{i,eq}(r)\nabla\mu_i(\mathbf{r},t) + \frac{w_{i,eq}(r)}{w_{T,eq}(r)}\left\{\eta\nabla^2\mathbf{v}(\mathbf{r},t) + \gamma\nabla\left[\nabla\cdot\mathbf{v}(\mathbf{r},t)\right]\right\} \\ &\mp L\left[\mathbf{v}_1(\mathbf{r},t)-\mathbf{v}_2(\mathbf{r},t)\right],\end{aligned} \tag{5.7}$$

where the upper and lower signs in Eq. (5.7) are used for $i = 1$ and 2, respectively. I derived Eq. (5.7) using the relation $\nabla P(\mathbf{r},t) = \sum_i^2\{w_i(\mathbf{r},t)\nabla\mu_i(\mathbf{r},t) - w_i(\mathbf{r},t)\nabla\phi_i(r)/m_i\}$. Equation (5.7) was linearlized by substituting the equilibrium mass-density field of solvent i, $w_{i,eq}(r)$ for $w_i(\mathbf{r},t)$. Since the velocity is small, I omitted the nonlinear terms.

The hydrodynamic equation (5.7) gives the long-wavelength limit of the microscopic equation (5.2). The first term of the right-hand side in Eq. (5.7) is in agreement with the first term in Eq. (5.2). The second and third terms in Eq. (5.7) correspond to the term including $\mathbf{M}_{ij}(t-t', \mathbf{r}, \mathbf{r}')$ in Eq. (5.2) in the long-wavelength limit. Then, applying the long-wavelength limit approximation to $\mathbf{M}_{ij}(t-t', \mathbf{r}, \mathbf{r}')$, the basic equations for a binary solvent in the steady state are obtained as follows:

$$\nabla \cdot w_{i,eq}(r)\mathbf{v}_i(\mathbf{r}) = 0, \tag{5.8}$$

$$-w_{i,eq}(r)\nabla\mu_i(\mathbf{r}) + \frac{w_{i,eq}(r)}{w_{T,eq}(r)}\left\{\eta\nabla^2\mathbf{v}(\mathbf{r}) + \gamma\nabla\left[\nabla\cdot\mathbf{v}(\mathbf{r})\right]\right\} \mp L\left[\mathbf{v}_1(\mathbf{r}) - \mathbf{v}_2(\mathbf{r})\right] = 0, \tag{5.9}$$

for $i = 1$ and 2. Equation (5.8) includes $w_{i,eq}(r)$ instead of $w_i(\mathbf{r}, t)$ for the same reason as for Eq. (5.7). The argument t in all functions was omitted because of the steady state. Assuming the slip boundary condition on the solute surface ($r = R_a$), I solve the basic equations Eqs. (5.8) and (5.9).

5.2 Symmetries of solutions

I rewrite the chemical potential $\mu_i(\mathbf{r})$ in Eq. (5.9) using the function $\mathcal{P}_i(\mathbf{r}) \equiv w_{i,eq}(r)\mu_i(\mathbf{r})$. Since the basic equations Eqs. (5.8) and (5.9) are linearized, the solutions $\mathcal{P}_i(\mathbf{r})$ and $\mathbf{v}_i(\mathbf{r})$ are proportional to $\mathbf{u}$. Owing to the spherical symmetry of the solute-solvent i potential, $\mathcal{P}_i(\mathbf{r})$ and $\mathbf{v}_i(\mathbf{r})$ included in the basic equations are described as follows:

$$\mathcal{P}_i(\mathbf{r}) = P_i(r)(\hat{\mathbf{r}}\cdot\mathbf{u}), \tag{5.10}$$

$$\mathbf{v}_i(\mathbf{r}) = v_{\hat{r},i}(r)(\hat{\mathbf{r}}\cdot\mathbf{u})\hat{\mathbf{r}} + v_{u,i}(r)\mathbf{u}. \tag{5.11}$$

Here, $\hat{\mathbf{r}}$ is the unit vector in the $\mathbf{r}$ direction.

Substituting these expressions (5.10), (5.11) into eqs. (5.8) and (5.9), the basic

equations are rewritten as

$$\frac{d}{dr}\{w_{i,eq}(r)v_{\hat{r},i}(r)\}+\frac{2w_{i,eq}(r)v_{\hat{r},i}(r)}{r}+\frac{d}{dr}\{w_{i,eq}(r)v_{u,i}(r)\}=0, \tag{5.12}$$

$$-\frac{P_i(r)}{r}+\frac{w_{i,eq}(r)}{w_{T,eq}(r)}\left[\eta\left\{\frac{2v_{\hat{r}}(r)}{r^2}+\frac{2}{r}\frac{dv_u(r)}{dr}+\frac{d^2v_u(r)}{dr^2}\right\}\right.$$
$$\left.+\gamma\left\{\frac{2v_{\hat{r}}(r)}{r^2}+\frac{1}{r}\frac{dv_{\hat{r}}(r)}{dr}+\frac{1}{r}\frac{dv_u(r)}{dr}\right\}\right]\mp L(v_{u,1}(r)-v_{u,2}(r))=0, \tag{5.13}$$

$$-w_{i,eq}(r)\frac{d}{dr}\frac{P_i(r)}{rw_{i,eq}(r)}+\frac{w_{i,eq}(r)}{w_{T,eq}(r)}\left[\eta\left\{6\frac{d}{dr}\frac{v_{\hat{r}}(r)}{r^2}+r\frac{d^2}{dr^2}\frac{v_{\hat{r}}(r)}{r^2}\right\}\right.$$
$$\left.+\gamma\left\{5\frac{d}{dr}\frac{v_{\hat{r}}(r)}{r^2}+r\frac{d^2}{dr^2}\frac{v_{\hat{r}}(r)}{r^2}-\frac{1}{r^2}\frac{dv_u(r)}{dr}+\frac{1}{r}\frac{d^2v_u(r)}{dr^2}\right\}\right]\mp L(\frac{v_{\hat{r},1}(r)}{r}-\frac{v_{\hat{r},2}(r)}{r})=0. \tag{5.14}$$

Here, $v_u(r)=\sum_i w_{i,eq}(r)v_{u,i}(r)/w_{T,eq}(r)$ and $v_{\hat{r}}(r)=\sum_i w_{i,eq}(r)v_{\hat{r},i}(r)/w_{T,eq}(r)$.

5.3 Perturbation expansions

I expand the basic equations (5.12), (5.13) and (5.14) in powers of the ratio between the solute and solvent size

$$\epsilon\equiv\frac{b}{R_a}. \tag{5.15}$$

If particles of the two-component solvent have different sizes, b is the radius of a larger solvent particle. As is the case for the one-component solvent system, I divide the whole space into two regions: the outer region far away from the solute and the boundary region near the solute. The outer region is defined by the region where $w_{1,eq}(r)=\rho_1$ and $w_{2,eq}(r)=\rho_2$. The boundary layer is defined by the region where $w_{1,eq}(r)\neq\rho_1$ or $w_{2,eq}(r)\neq\rho_2$. In each of the two regions, I expand the basic equations.

Since the boundary layer is dominated by the scale of the solvent particle size, I introduce a stretched variable $x\equiv(r-R_a)/b$. Here, $w_{i,eq}(r)$ is assumed to be represented by the function of x, $w_{i,e}(x)$. With the new variable x being fixed, the solutions of Eqs. (5.12) - (5.14) are expanded as $v_{\hat{r},i}(r)=\sum_{n=0}^{\infty}\epsilon^n v_{\hat{r},i,b}^{(n)}(x)$, $v_{u,i}(r)=\sum_{n=0}^{\infty}\epsilon^n v_{u,i,b}^{(n)}(x)$, and $R_aP_i(r)=\sum_{n=0}^{\infty}\epsilon^n P_{i,b}^{(n)}(x)$. In addition, excluding the length scale R_a or b explicitly, I assume that the coefficient L scales $\bar{L}=R_a^2L$.

When solving the basic equations (5.12), (5.13) and (5.14), the slip boundary condition is assumed on the solute surface. The boundary condition for the expansion

of $v_{u,b}(r)$ is given as

$$\left.\frac{dv_{u,b}^{(n+1)}(x)}{dx}\right|_{x=0} = v_{u,b}^{(n)}(0). \tag{5.16}$$

In the outer region, Eqs. (5.8) and (5.9) reduce to the same expressions as the incompressible hydrodynamic equations,

$$\nabla \cdot \mathbf{v}(\mathbf{r}) = 0, \tag{5.17}$$

$$-\nabla P(\mathbf{r}) + \eta \nabla^2 \mathbf{v}(\mathbf{r}) = 0. \tag{5.18}$$

Equation (5.17) is obtained by the summation of Eq. (5.8) for $i = 1$ and 2. Equation (5.18) is also obtained by the same summation using the relation $\nabla P(\mathbf{r}, t) = \sum_i^2 \{w_i(\mathbf{r}, t)\nabla\mu_i(\mathbf{r}, t)\}$. Since the outer region is dominated by the scale of the solute particle size, the solutions of Eqs. (5.17) and (5.18) are expanded as $v_{\hat{r},i}(r) = \sum_{n=0}^{\infty} \epsilon^n v_{\hat{r},i,o}^{(n)}(\bar{r})$, $v_{u,i}(r) = \sum_{n=0}^{\infty} \epsilon^n v_{u,i,o}^{(n)}(\bar{r})$, and $R_a P_i(r) = \sum_{n=0}^{\infty} \epsilon^n P_{i,o}^{(n)}(\bar{r})$, with the variable $\bar{r} \equiv r/R_a$ fixed.

Since the perturbation expansions are applied independently in two regions, I impose the same connecting condition as that given by Eqs. (3.22) - (3.24) for the solutions $v_{\hat{r},i}(r)$, $v_{u,i}(r)$, and $P_i(\mathbf{r})$. Using the connecting condition, as is the case of the one-component solvent system, the boundary layer solutions provide the boundary conditions of the outer solutions at $\bar{r} = 1$. The procedure of derivation of the boundary conditions has some similarities to the one-component case.[40]

5.3.1 Equations of terms proportional to ϵ^0

Substituting the expansions of $v_{\hat{r},i}(r)$, $v_{u,i}(r)$, and $P_i(\mathbf{r})$, into the equation of motion given by Eq. (5.13) with $\epsilon = 0$, I obtain

$$\eta \frac{w_{i,e}(x)}{w_{T,e}(x)} \frac{d^2 v_{u,b}^{(0)}(x)}{dx^2} = 0. \tag{5.19}$$

Since $w_{i,e}(x) \neq 0$, I derive

$$\frac{d^2 v_{u,b}^{(0)}(x)}{dx^2} = 0. \tag{5.20}$$

Using Eq. (3.24), the solution of Eq. (5.20) is

$$v_{u,b}^{(0)}(x) = A, \tag{5.21}$$

where A is the integral constant. Under the connecting condition given by Eq. (3.22) with $n = m = 0$, I obtain

$$v_{u,b}^{(0)}(x) = v_{u,o}^{(0)}(1). \tag{5.22}$$

Terms proportional to ϵ^0 of the equation of motion given by Eq. (5.14) are

$$\frac{w_{i,e}(x)}{w_{T,e}(x)}\left[\eta\frac{d^2v^{(0)}_{\hat{r},b}(x)}{dx^2}+\gamma\left\{\frac{d^2v^{(0)}_{\hat{r},b}(x)}{dx^2}+\frac{d^2v^{(0)}_{u,b}(x)}{dx^2}\right\}\right]=0. \tag{5.23}$$

Substituting Eq. (5.21) into Eq. (5.23), I obtain

$$(\eta+\gamma)\frac{d^2v^{(0)}_{\hat{r},b}(x)}{dx^2}=0. \tag{5.24}$$

In the same way as for Eq. (5.22), the solution of Eq. (5.24) is derived as

$$v^{(0)}_{\hat{r},b}(x)=v^{(0)}_{\hat{r},o}(1). \tag{5.25}$$

Terms proportional to ϵ^0 of the continuity equation given by Eq. (5.12) are

$$\frac{d}{dx}\{w_{i,e}(x)v^{(0)}_{\hat{r},i,b}(x)\}+\frac{d}{dx}\{w_{i,e}(x)v^{(0)}_{u,i,b}(x)\}=0. \tag{5.26}$$

The summation of Eq. (5.26) at $i=1$ and 2 is

$$\frac{d}{dx}\{w_{T,e}(x)(v^{(0)}_{\hat{r},b}(x)+v^{(0)}_{u,b}(x))\}=0. \tag{5.27}$$

Substituting Eqs. (5.22) and (5.25) into Eq. (5.27), one can derive the boundary condition proportional to ϵ^0 as

$$v^{(0)}_{\hat{r},b}(x)+v^{(0)}_{u,b}(x)=v^{(0)}_{\hat{r},o}(1)+v^{(0)}_{u,o}(1)=0. \tag{5.28}$$

5.3.2 Equations of terms proportional to ϵ^1

Terms proportional to ϵ of Eq. (5.13) are

$$\frac{w_{i,e}(x)}{w_{T,e}(x)}\left[\eta\left\{\frac{d^2v^{(1)}_{u,b}(x)}{dx^2}+2\frac{dv^{(0)}_{u,b}(x)}{dx}+\right\}+\gamma\left\{\frac{dv^{(0)}_{\hat{r},b}(x)}{dx}+\frac{dv^{(0)}_{u,b}(x)}{dx}\right\}\right]=0. \tag{5.29}$$

The substitution of Eqs. (5.22) and (5.25) into Eq. (5.29) gives

$$\eta\frac{d^2v^{(1)}_{u,b}(x)}{dx^2}=0. \tag{5.30}$$

Using the connecting condition given by Eq. (3.22), I derive the solution of Eq. (5.30) as

$$v^{(1)}_{u,b}(x)=\left.\frac{dv^{(0)}_{u,o}(\bar{r})}{d\bar{r}}\right|_{\bar{r}=1}x+v^{(1)}_{u,o}(1). \tag{5.31}$$

Since Eq. (5.16) at $n = 0$ gives

$$\left.\frac{dv_{u,b}^{(1)}(x)}{dx}\right|_{x=0} = v_{u,b}^{(0)}(0), \tag{5.32}$$

using Eqs. (5.22) and (5.31), I derive the boundary condition proportional to ϵ^0 as

$$\left.\frac{dv_{u,o}^{(0)}(\bar{r})}{d\bar{r}}\right|_{\bar{r}=1} = v_{u,o}^{(0)}(1). \tag{5.33}$$

Since terms proportional to ϵ in Eq. (5.12) are

$$\frac{d}{dx}\left[w_{i,e}(x)\left\{v_{\hat{r},i,b}^{(1)}(x) + v_{u,i,b}^{(1)}(x)\right\}\right] + 2w_{i,e}(x)v_{\hat{r},i,b}^{(0)}(x) = 0, \tag{5.34}$$

the summation of Eq. (5.34) at $i = 1$ and 2 is

$$\frac{d}{dx}\left[w_{T,e}(x)\left\{v_{\hat{r},b}^{(1)}(x) + v_{u,b}^{(1)}(x)\right\}\right] + 2w_{T,e}(x)v_{\hat{r},b}^{(0)}(x) = 0. \tag{5.35}$$

Using Eqs. (5.25) and (5.33), I derive the solution of Eq. (5.35) as

$$v_{\hat{r},b}^{(1)}(x) + v_{u,b}^{(1)}(x) = \frac{2v_{u,o}^{(0)}(1)}{w_{T,e}(x)}\int_0^x w_{T,e}(x')dx' + \frac{B}{w_{T,e}(x)}, \tag{5.36}$$

where B is the integral constant. Since $w_{T,e}(0) = 0$, I find $B = 0$ under the condition that the velocity fields do not diverge at $x \to 0$.

The asymptotic form of Eq. (5.36) is represented as

$$v_{\hat{r},b}^{(1)}(x) + v_{u,b}^{(1)}(x) = \left.\frac{d}{d\bar{r}}\left\{v_{\hat{r},o}^{(0)}(\bar{r}) + v_{u,o}^{(0)}(\bar{r})\right\}\right|_{\bar{r}=1} x + v_{\hat{r},o}^{(1)}(1) + v_{u,o}^{(1)}(1) \text{ for } x \to \infty. \tag{5.37}$$

Thus, the boundary condition for $v_{\hat{r},o}^{(1)}(\bar{r}) + v_{u,o}^{(1)}(\bar{r})$ is given by the constant term of Eq. (5.36) at $x \to \infty$, that is,

$$v_{\hat{r},o}^{(1)}(1) + v_{u,o}^{(1)}(1) = \alpha v_{u,o}^{(0)}(1) \tag{5.38}$$

where

$$\alpha = \frac{2}{w_{T,e}(\infty)}\int_0^\infty \{w_{T,e}(x') - w_{T,e}(\infty)\}dx'. \tag{5.39}$$

Here, $w_{T,e}(\infty) = w_1 + w_2 (\equiv w_T)$.

Terms proportional to ϵ in Eq. (5.14) are

$$-w_{i,e}(x)\frac{d}{dx}\frac{P_{i,b}^{(0)}(x)}{w_{i,e}(x)}+\frac{w_{i,e}(x)}{w_{T,e}(x)}\left[\eta\left\{\frac{d^2v_{\hat{r},b}^{(1)}(x)}{dx^2}-x\frac{d^2v_{\hat{r},b}^{(0)}(x)}{dx^2}+2\frac{dv_{\hat{r},b}^{(0)}(x)}{dx}\right\}\right.$$
$$\left.+\gamma\left\{-x\frac{d^2v_{\hat{r},b}^{(0)}(x)}{dx^2}+\frac{d^2v_{\hat{r},b}^{(1)}(x)}{dx^2}+\frac{dv_{\hat{r},b}^{(0)}(x)}{dx}-x\frac{d^2v_{u,b}^{(0)}(x)}{dx^2}+\frac{d^2v_{u,b}^{(1)}(x)}{dx^2}-\frac{dv_{u,b}^{(0)}(x)}{dx}\right\}\right]=0. \tag{5.40}$$

The substitution of Eqs. (5.22), (5.25) and (5.30) gives

$$-w_{i,e}(x)\frac{d}{dx}\frac{P_{i,b}^{(0)}(x)}{w_{i,e}(x)}+(\eta+\gamma)\frac{w_{i,e}(x)}{w_{T,e}(x)}\frac{d^2v_{\hat{r},b}^{(1)}(x)}{dx^2}=0. \tag{5.41}$$

Since $v_{\hat{r},b}^{(1)}(x)$ is derived from Eqs. (5.31) and (5.36), I can derive $P_{i,b}^{(0)}(x)$ by solving Eq. (5.41). The derivation of $P_{i,b}^{(0)}(x)$, however, requires consideration when binary solvent particles have different sizes. Details are given in Chap. 5.3.4.

5.3.3 Equations of terms proportional to ϵ^2

I derive the boundary condition for $v_{u,o}^{(1)}(\bar{r})$ using terms proportional to ϵ^2 in Eq. (5.13). According to Eq. (3.22), the boundary condition is obtained from the differential of $v_{u,b}^{(2)}(x)$. I obtain the differential of $v_{u,b}^{(2)}(x)$ by integrating the second-order differential of $v_{u,b}^{(2)}(x)$, which is included in terms proportional to ϵ^2 in Eq. (5.13).

The boundary condition for $v_{u,o}^{(1)}(\bar{r})$ is obtained from f defined by

$$f\equiv\lim_{x\to\infty}\left[\frac{dv_{u,b}^{(2)}(x)}{dx}-Cx\right]-\left.\frac{dv_{u,b}^{(2)}(x)}{dx}\right|_{x=0}, \tag{5.42}$$

where $C=\lim_{x\to\infty}d^2v_{u,b}^{(2)}(x)/dx^2$. Since $\left.dv_{u,b}^{(2)}(x)/dx\right|_{x=0}=v_{u,b}^{(1)}(0)$ is obtained from Eq. (5.16), using Eq. (5.31) at $x=0$, I derive

$$\left.\frac{dv_{u,b}^{(2)}(x)}{dx}\right|_{x=0}=v_{u,o}^{(1)}(1). \tag{5.43}$$

Using Eq. (3.22), the asymptotic form of $dv_{u,b}^{(2)}(\bar{x})/dx$ is

$$\lim_{x\to\infty}\frac{dv_{u,b}^{(2)}(\bar{x})}{dx}=\left.\frac{d^2v_{u,o}^{(0)}(\bar{r})}{d\bar{r}^2}\right|_{\bar{r}=1}x+\left.\frac{dv_{u,o}^{(1)}(\bar{r})}{d\bar{r}}\right|_{\bar{r}=1}. \tag{5.44}$$

Thus, from Eqs. (5.43) and (5.44), I derive

$$\left.\frac{dv_{u,o}^{(1)}(\bar{r})}{d\bar{r}}\right|_{\bar{r}=1} - v_{u,o}^{(1)}(1) = f. \tag{5.45}$$

Equation (5.42) is rewritten as

$$f = \int_0^\infty \left(\frac{d^2 v_{u,b}^{(2)}(x)}{dx^2} - C \right) dx. \tag{5.46}$$

I obtain the second-order differential of $v_{u,o}^{(2)}(x)$ from terms proportional to ϵ^2 of Eq. (5.13) as

$$\begin{aligned} -P_{i,b}^{(0)}(x) + \frac{w_{i,e}(x)}{w_{T,e}(x)} \Bigg[\eta \left\{ 2v_{\hat{r},b}^{(0)}(x) + \frac{d^2 v_{u,b}^{(2)}(x)}{dx^2} - 2x\frac{dv_{u,b}^{(0)}(x)}{dx} + 2\frac{dv_{u,b}^{(1)}(x)}{dx} \right\} \\ + \gamma \left\{ -x\frac{dv_{\hat{r},b}^{(0)}(x)}{dx} + \frac{dv_{\hat{r},b}^{(1)}(x)}{dx} + 2v_{\hat{r},b}^{(0)}(x) - x\frac{dv_{u,b}^{(0)}(x)}{dx} + \frac{dv_{u,b}^{(1)}(x)}{dx} \right\} \Bigg] = 0. \end{aligned} \tag{5.47}$$

Summing up of Eq. (5.47) at $i = 1$ and 2 and using Eqs. (5.22), (5.25) and (5.31), f is

$$\begin{aligned} f = & \frac{1}{\eta} \int_0^\infty \Big\{ (P_{1,b}^{(0)}(x) + P_{2,b}^{(0)}(x)) - (P_{1,b}^{(0)}(\infty) + P_{2,b}^{(0)}(\infty)) \\ & -\gamma \frac{dv_{\hat{r},b}^{(1)}(x)}{dx} + \gamma \left.\frac{dv_{\hat{r},b}^{(1)}(x)}{dx}\right|_{x=\infty} \Big\} dx. \end{aligned} \tag{5.48}$$

Substituting $v_{\hat{r},b}^{(1)}(x)$ obtained from Eqs. (5.30) and (5.36) and $P_{i,b}^{(0)}(x)$ derived from Eq. (5.41), I obtain the boundary condition for $v_{u,o}^{(1)}(\bar{r})$ as

$$\left.\frac{dv_{u,o}^{(1)}(\bar{r})}{d\bar{r}}\right|_{\bar{r}=1} - v_{u,o}^{(1)}(1) = \frac{\alpha}{2\eta} P_o^{(0)}(1) - \beta v_{u,o}^{(0)}(1). \tag{5.49}$$

Here,

$$\begin{aligned}\beta =& \int_0^{x_0} \Delta \mathrm{v}_1(x)dx + \int_{x_0}^{\infty} \Delta \mathrm{v}_T(x)dx \\ & - \left(1+\frac{\gamma}{\eta}\right)\left\{\int_0^{x_0} w_1(x)\int_x^{x_0}\frac{w_1'(x')}{w_1^2(x')}\Delta \mathrm{v}_1(x')dx'dx \right. \\ & \left. + \int_{x_0}^{\infty} w_T(x)\int_x^{\infty}\frac{w_T'(x')}{w_T^2(x')}\Delta \mathrm{v}_T(x')dx'dx\right\} \\ & - \left(1+\frac{\gamma}{\eta}\right)\int_0^{x_0} w_1(x)dx\left\{\int_{x_0}^{\infty}\frac{w_T'(x)}{w_T^2(x)}\Delta \mathrm{v}_T(x)dx \right. \\ & \left. + \Delta \mathrm{v}_1(x_0)\left(\frac{1}{w_1(x_0)}-\frac{1}{w_T(x_0)}\right)\right\}, \end{aligned} \tag{5.50}$$

where

$$\Delta \mathrm{v}_j(x) = \frac{2w_j'(x)}{w_j^2(x)}\int_0^x w_j(x')dx', \tag{5.51}$$

$$w_j'(x) = \frac{dw_j(x)}{dx}, \tag{5.52}$$

for $j = 1$ or T. Here, $x_0 = (b-a)/a$. The subscript e in the equilibrium mass density field was omitted for simplicity.

5.3.4 Derivation of $P_{i,b}^{(0)}(x)$

When binary solvent particles have different sizes ($a < b$), one needs special consideration to derive Eq. (5.50). In Eq. (5.41), $v_{\hat{r},b}^{(1)}(x)$ changes abruptly at $r = R+b$ or $x = (b-a)/b\,(\equiv x_0)$ because $w_{2,e}(x)$ vanishes abruptly for $r < R+b$ or $x < x_0$. The differential of $v_{\hat{r},b}^{(1)}(x)$ at $x = x_0$ causes an extremely large $P_{i,b}^{(0)}(x)$. Thus, solving Eq. (5.41) except for $x = x_0$, I derive $P_{i,b}^{(0)}(x)$.

When $x_0 < x$, solving Eq. (5.41), I obtain

$$\begin{aligned}P_{i,b}^{(0)}(x) =& w_{i,e}(x)\frac{P_{i,o}^{(0)}(1)}{w_{i,e}(\infty)} \\ & - (\eta+\gamma)w_{i,e}(x)\int_x^{\infty}\frac{1}{w_{T,e}(x')}\frac{d^2}{dx'^2}\left\{\frac{2v_{u,o}^{(0)}(1)}{w_{T,e}(x')}\int_0^{x'} w_{T,e}(x'')dx''\right\}dx', \end{aligned} \tag{5.53}$$

where I use $P^{(0)}_{i,b}(\infty) = P^{(0)}_{i,o}(1)$. In the region $x < x_0$,

$$P^{(0)}_{1,b}(x) = w_{1,e}(x) \lim_{x\to x_o^-} \frac{P^{(0)}_{1,b}(x)}{w_{1,e}(x)} - (\eta+\gamma) w_{1,e}(x) \int_x^{x_0} \frac{1}{w_{1,e}(x')} \frac{d^2}{dx'^2} \left\{ \frac{2v^{(0)}_{u,o}(1)}{w_{1,e}(x')} \int_0^{x'} w_{1,e}(x'')dx'' \right\} dx'. \tag{5.54}$$

Here, $x \to x_0^-$ indicates that x approaches x_0 from values less than x_0.

To obtain the value of $\lim_{x\to x_o^-}\{P^{(0)}_{1,b}(x)/w_{1,e}(x)\}$ in Eq. (5.54), I examine the boundary condition of $P^{(0)}_{1,b}(x)/w_{1,e}(x)$ at $x = x_0$. Integrating Eq. (5.41) at $i = 1$ from $x_0 - \delta x$ to $x_0 + \delta x$, where $\delta x > 0$, I obtain

$$-\int_{x_0-\delta x}^{x_0+\delta x} \frac{d}{dx}\frac{P^{(0)}_{1,b}(x)}{w_{1,e}(x)}dx + (\eta+\gamma)\int_{x_0-\delta x}^{x_0+\delta x} \left\{ \frac{1}{w_{T,e}(x)} \frac{d^2}{dx^2} \left[v^{(1)}_{\hat{r},b}(x) + v^{(1)}_{u,b}(x) \right] \right\} dx = 0. \tag{5.55}$$

To derive Eq. (5.55), I have used Eq. (5.30). Equation (5.55) is rewritten as

$$-\int_{x_0-\delta x}^{x_0+\delta x} \frac{d}{dx}\frac{P^{(0)}_{1,b}(x)}{w_{1,e}(x)}dx + (\eta+\gamma)\int_{x_0-\delta x}^{x_0+\delta x} \frac{d}{dx}\left\{ \frac{1}{w_{T,e}(x)} \frac{d}{dx} \left[v^{(1)}_{\hat{r},b}(x) + v^{(1)}_{u,b}(x) \right] \right\} - (\eta+\gamma)\int_{x_0-\delta x}^{x_0+\delta x} \frac{d}{dx}\left[\frac{1}{w_{T,e}(x)}\right] \frac{d}{dx}\left[v^{(1)}_{\hat{r},b}(x) + v^{(1)}_{u,b}(x) \right] dx = 0. \tag{5.56}$$

When $\delta x \to 0$,

$$-\left[\frac{P^{(0)}_{1,b}(x)}{w_{1,e}(x)}\right]_{x_0^-}^{x_0^+} + (\eta+\gamma)\left[\frac{1}{w_{T,e}(x)}\frac{d}{dx}\left[v^{(1)}_{\hat{r},b}(x) + v^{(1)}_{u,b}(x) \right]\right]_{x_0^-}^{x_0^+} - (\eta+\gamma)\left[\frac{1}{w_{T,e}(x)}\right]_{x_0^-}^{x_0^+} \frac{d}{dx}\left[v^{(1)}_{\hat{r},b}(x) + v^{(1)}_{u,b}(x) \right]\Big|_{x=x_0} = 0, \tag{5.57}$$

where $[Z(x)]_{x_0^-}^{x_0^+} \equiv \lim_{x\to x_0^+} Z(x) - \lim_{x\to x_0^-} Z(x)$. To derive Eq. (5.57), I have used

$$\frac{d}{dx}\frac{1}{w_{T,e}(x)} = \left[\frac{1}{w_{T,e}(x)}\right]_{x_0^-}^{x_0^+} \delta(x - x_0). \tag{5.58}$$

I obtain the value of $\lim_{x\to x_o^-}\{P^{(0)}_{1,b}(x)/w_{1,e}(x)\}$ in Eq. (5.54), substituting the differential of $v^{(1)}_{\hat{r},1,b}(x) + v^{(1)}_{u,1,b}(x)$ instead of the differential of $v^{(1)}_{\hat{r},b}(x) + v^{(1)}_{u,b}(x)$ in Eq. (5.57). This is because the differential of $v^{(1)}_{\hat{r},b}(x) + v^{(1)}_{u,b}(x)$ at $x = x_0$ cannot be

defined owing to the discontinuity of $v^{(1)}_{\hat{r},b}(x)+v^{(1)}_{u,b}(x)$ at $x=x_0$. Thus, Eq. (5.57) is rewritten as

$$-\left[\frac{P^{(0)}_{1,b}(x)}{w_{1,e}(x)}\right]^{x_0^+}_{x_0^-}+(\eta+\gamma)\left[\frac{1}{w_{T,e}(x)}\frac{d}{dx}\left[v^{(1)}_{\hat{r},b}(x)+v^{(1)}_{u,b}(x)\right]\right]^{x_0^+}_{x_0^-}$$
$$-(\eta+\gamma)\left[\frac{1}{w_{T,e}(x)}\right]^{x_0^+}_{x_0^-}\frac{d}{dx}\left[v^{(1)}_{\hat{r},1,b}(x)+v^{(1)}_{u,1,b}(x)\right]\Bigg|_{x=x_0}=0. \tag{5.59}$$

Note that $v^{(1)}_{\hat{r},b}(x)+v^{(1)}_{u,b}(x)$ is in agreement with $v^{(1)}_{\hat{r},1,b}(x)+v^{(1)}_{u,1,b}(x)$ for $x<x_0$, since $w_{2,e}(x)=0$. Using Eq. (5.59), I obtain $P^{(0)}_{1,b}(x)$ for $x<x_0$ from Eq. (5.54). Substituting $P^{(0)}_{1,b}(x)$ derived from Eqs. (5.53) and (5.54) in Eq. (5.48), I obtain Eqs. (5.49) - (5.52).

5.4 Boundary conditions of outer region

From Eqs. (5.33) and (5.38), by omitting terms higher than the second order of ϵ, the boundary condition for $v_{\hat{r},o}(\bar{r})+v_{u,o}(\bar{r})$ is rewritten as

$$v_{\hat{r}}(R_a)+v_u(R_a)=\epsilon\alpha v_u(R_a). \tag{5.60}$$

Substituting $x=(r-R_a)/b$ into Eq. (5.39),

$$\epsilon\alpha=\frac{2}{R+a}\int_{R+a}^{\infty}\left[\frac{w_T(r)}{w_T(\infty)}-1\right]dr. \tag{5.61}$$

From Eqs (5.36) and (5.49), the boundary condition for $v_{u,o}(\bar{r})$ is rewritten as

$$\left.\frac{dv_u(r)}{dr}\right|_{r=R_a}=\frac{1-\epsilon\beta}{R_a}v_u(R_a)+\frac{\epsilon\alpha}{2\eta}P_s(R_a). \tag{5.62}$$

The parameter β is given by

$$\begin{aligned}\epsilon\beta=&\frac{1}{R+a}\left\{\int_{R+a}^{R+b}\Delta v_1(r)dr+\int_{R+b}^{\infty}\Delta v_T(r)dr\right.\\
&-\left(1+\frac{\gamma}{\eta}\right)\left[\int_{R+a}^{R+b}w_1(r)\int_r^{R+b}\frac{\omega_1(r')}{w_1(r')}\Delta v_1(r')dr'dr\right.\\
&\left.+\int_{R+b}^{\infty}w_T(r)\int_r^{\infty}\frac{\omega_T(r')}{w_T(r')}\Delta v_T(r')dr'dr\right]\\
&-\left(1+\frac{\gamma}{\eta}\right)\int_{R+a}^{R+b}w_1(r)dr\left[\int_{R+b}^{\infty}\frac{\omega_T(r)}{w_T(r)}\Delta v_T(r)dr\right.\\
&\left.\left.+\Delta v_1(R+b)\left(\frac{1}{w_1(R+b)}-\frac{1}{w_T(R+b)}\right)\right]\right\},\end{aligned} \tag{5.63}$$

where

$$\Delta v_j(r) = \frac{2\omega_j(r)}{w_j(r)} \int_{R+a}^{r} w_j(r')dr', \tag{5.64}$$

$$\omega_j(r) = \frac{1}{w_j(r)} \frac{dw_j(r)}{dr}, \tag{5.65}$$

for $j = 1$ or T. I obtain Eqs. (5.63) - (5.65) substituting $x = (r - R_a)/b$ into Eqs. (5.50) - (5.52). I omitted the subscript eq in the equilibrium mass density fields for simplicity. Although the slip boundary condition holds at $\epsilon = 0$, Eq. (5.62) deviates from the slip condition when $\epsilon \neq 0$. Note that the third term including L in Eq. (5.9) does not affect the boundary conditions because the coefficient L is assumed to be proportional to ϵ^2.

Although Eqs. (5.60) and (5.62) are the same expressions as those obtained in the one-component solvent system Eqs. (5.17) and (5.18), the parameters α and β given by Eqs. (5.61) and (5.63) are different from those of the one-component system. These parameters α and β depend on the equilibrium mass density fields of a binary solvent mixture, $w_1(r)$ and $w_2(r)$. In addition, α and β depend on the size of the particles, when the sizes of binary solvent particles are different. Note that the expressions of α and β reduces those of the one-component system when the the density of the second component $w_2(r)$ is zero ($w_T(r) = w_1(r)$).

5.5 Drag coefficient

Solving Eqs. (5.17) and (5.18) with the derived boundary conditions Eqs. (5.60) and (5.62), I obtain the drag coefficient. Since these equations are the same as those derived in a one-component system, the expression of the drag coefficient is the same as Eqs. (4.6) and (4.8):

$$\xi = c\pi\eta R_a, \tag{5.66}$$

$$c = \frac{48 - 24\epsilon\alpha - 24\epsilon\beta}{12 - 4\epsilon\beta + (\epsilon\alpha)^2}. \tag{5.67}$$

The parameters α and β are given by Eqs. (5.61) and (5.63), respectively. From the drag coefficient ξ, the diffusion coefficient is obtained through the Einstein relation $D = k_B T/\xi$.

5.6 Summary and Discussion

I have formulated a theory of the drag coefficient in a binary solvent mixture, extending the perturbation theory for a one-component solvent system. I expanded the generalized Langevin equations for a two-component fluid with respect to the size ratio between the solute and solvent particles. The expansion allowed one to derive hydrodynamic equations with the boundary conditions depending on the density distribution of a binary solvent mixture. The derived boundary condition shows that the slip boundary condition breaks down owing to the solvation structure of a binary mixture. Solving hydrodynamic equations with the boundary conditions, I obtained an analytical expression of the drag coefficient of a large solute.

The present theory is distinct from that of the one-component solvent system in the boundary conditions. The parameters α and β included in the boundary conditions are given by the expressions different from those of a one-component system. In contrast, I derived the same hydrodynamic equations as those of a one-component solvent system. Thus, the analytical expressions of the drag coefficient (5.66) and (5.67) are identical with that of a one-component system, although the expressions of α and β in Eq. (5.67) are different.

Chapter 6

Application of the theory to binary hard-sphere system

In the previous chapter, I formulated the perturbation theory for the drag coefficient in a binary mixture. The drag coefficient is calculated by solving the hydrodynamic equations and boundary conditions on the solute surface. I showed that the boundary condition is determined by the solvation structure of a binary mixture. The perturbation theory can be applied to the system in which the particles interact with spherically symmetric potentials. In this chapter, applying the perturbation theory to a binary hard-sphere system,[75] I investigate the solvation effect on the boundary conditions.

6.1 Calculation details

The system is composed of a large hard-sphere solute and a binary mixture of small (solvent) and medium-size (cosolvent) hard spheres. The radius of the solute sphere R is $50a$, where a is the radius of the solvent sphere. The radius of the cosolvent sphere b is varied from $2a$ to $6a$. The mass of the sphere is assumed to be proportional to the volume. Thus, the mass ratio of the solvent and cosolvent spheres is set to $1 : (b/a)^3$. The packing fraction of the cosolvent ϕ_2 is increased from 0.00 to 0.10 with the total packing fraction of the solvent and cosolvent being kept constant at 0.38.

I calculate the boundary condition coefficient c using Eq. (5.61), (5.63), and (5.67). The calculation requires the value of γ/η included in Eq. (5.63). Here, $\gamma = \eta/3+\zeta$, η is the shear viscosity, and ζ is the bulk viscosity. In this study, I assume for simplicity that the bulk viscosity is zero, that is, $\gamma = \eta/3$. In this case, since $\gamma/\eta = 1/3$, the

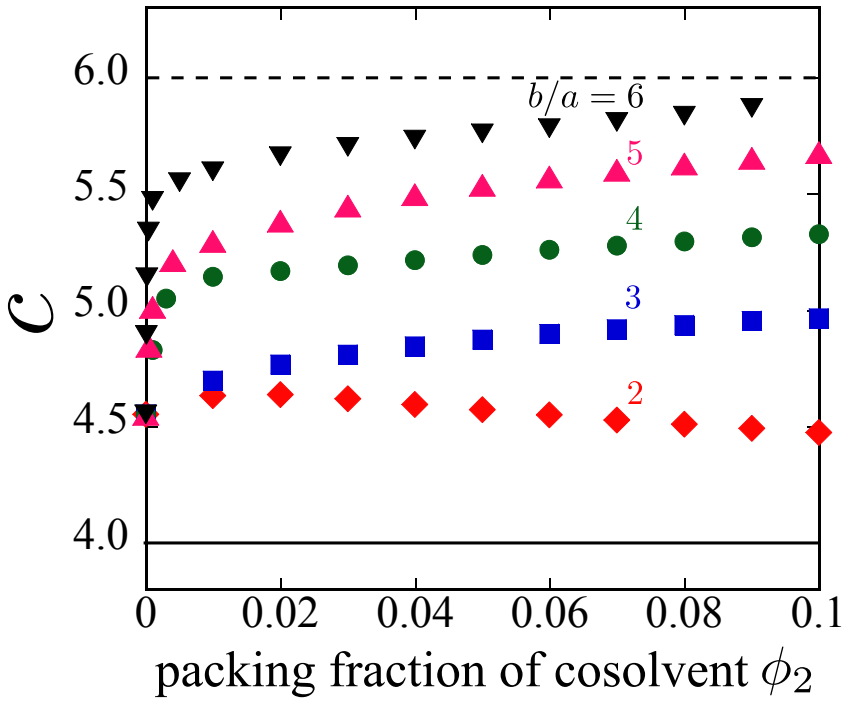

Figure 6.1 The boundary condition coefficient c as a function of the packing fraction of cosolvent spheres ϕ_2. The radius of the solute sphere is $50a$, where a is the radius of the solvent sphere. The radii of the cosolvent spheres b are $2a$ (diamonds), $3a$ (squares), $4a$ (circles), $5a$ (upward triangles), and $6a$ (downward triangles). Solid and dashed lines represent the slip ($c = 4$) and stick ($c = 6$) boundary conditions, respectively. The total packing fraction of the solvent and cosolvent is 0.38.

value of the shear viscosity is not required.

To calculate Eqs. (5.61) and (5.63), I also need the equilibrium mass density distributions, which are calculated from the radial distribution function $w_i(r) = \rho_i g_i(r)$. In this study, the radial distribution functions $g_i(r)$ are obtained using the OZ/HNC theory. For the numerical calculation, a hybrid convergence algorithm is employed.[66]–[71]

6.2 Results

6.2.1 Boundary conditions

The calculated results show that c have various values between 4 (the slip boundary condition) and 6 (the stick boundary condition) depending on the cosolvent radius

and cosolvent packing fraction (Fig. 6.1). As the cosolvent radius becomes larger, the value of c approaches the value of the stick boundary condition. For instance, c changes from 4.6 to 5.8 when the cosolvent radius increases from $2a$ to $6a$ at the same cosolvent packing fraction of 0.05. Note that c has a close value to the slip boundary condition in the case of the pure solvent ($\phi_2 = 0$), that is, $c = 4.5$.

When the cosolvent radius is larger than $3a$, the values of c increases as increasing the cosolvent packing fraction. In particular, when the cosolvent radius is larger than $4a$, c increases rapidly for a small amount of the cosolvent packing fraction. The increase is more rapidly as the cosolvent radius becomes larger. For instance, when $b = 6a$, $c = 5.4$ is obtained even at $\phi_2 = 0.005$. After the rapid increase, c gradually increases for larger cosolvent packing fractions.

In contrast to the case of $b \geq 3a$, when $b = 2a$, c has a value close to the slip boundary condition regardless of the cosolvent packing fraction. For $\phi_2 < 0.02$, c increases slightly with increasing cosolvent packing fraction. However, c decreases slowly for $\phi_2 > 0.02$. At $\phi_2 = 0.10$, the value of c is smaller than the value for the pure solvent. This decrease is not observed in the case of $b \geq 3a$.

6.2.2 Normalized equilibrium mass density fields

To clarify the dependence of c on the cosolvent packing fraction I consider the mass density field around the solute. Figure 6.2 shows the reduced mass density fields of the solvent $w_1(r)/\rho_T$ and cosolvent $w_2(r)/\rho_T$ when $b = 5a$. The high value of $w_1(r)/\rho_T$ and $w_2(r)/\rho_T$ represents the high mass density compared with the total bulk mass density $\rho_T \equiv \rho_1 + \rho_2$. In the present system, ρ_T is kept constant as the cosolvent packing fraction increases and the cosolvent radius changes.

The reduced mass density fields $w_1(r)/\rho_T$ and $w_2(r)/\rho_T$ have peaks at the solute surface where $r/a = 51$ and 55, respectively, when $b = 5a$ (Fig. 6.2). The peak of $w_2(r)/\rho_T$ grows considerably with increasing the cosolvent packing fraction. The value increases from 7.3 to 60.4 when the cosolvent packing fraction changes from 0.005 to 0.10. In contrast, the peak value of $w_1(r)/\rho_T$ slightly decreases with increasing the cosolvent packing fraction.

Since a high peak of the reduced mass density gives large values of β given by Eq. (5.63), c also has a large value through Eq. (5.67). Actually, at $b = 5a$, the value of c increases with the cosolvent packing fraction as with $w_2(r)/\rho_T$ (Fig. 6.1). Thus, the increase in c can be related to the increases in the peak of $w_2(r)/\rho_T$ when $b = 5a$.

I plot the dependence of the peak value of $w_2(R+b)/\rho_T$ and $w_1(R+a)/\rho_T$ on the cosolvent packing fraction in Fig. 6.3. The peak of $w_2(r)/\rho_T$ increases with increasing

cosolvent packing fraction and cosolvent sphere radius (Fig. 6.3 (a)). This behavior is the same as that observed in c when $b \geq 3a$. Then, the increase in c is correlated with the increase in the peak of $w_2(r)/\rho_T$ when $b \geq 3a$. The high peak gives large values of β included in c.

Using Eq. (5.67), I focus on the gradual increase in c for larger packing fractions observed when $b \geq 4a$. The parameter β included in Eq. (5.67) increases with the peak value of the mass density. From Eq. (5.67), one finds that c approaches asymptotically 6 with increasing β. Thus, even when the peak value of $w_2(r)/\rho_T$ greatly increases c increases gradually to 6.

The decrease in c at $b = 2a$ is correlated with the decrease in the peak value of $w_1(r)/\rho_T$. The peak value of $w_1(r)/\rho_T$ decreases slightly with increasing the cosolvent packing fraction (Fig. 6.3 (b)). It is considered that the decrease in c is caused by the decrease in β given by Eq. (5.63). Since the rate of increase in the peak of $w_2(r)/\rho_T$ is small at $b = 2a$, the value of β may decrease with decreasing in the peak of $w_1(r)/\rho_T$. In contrast, at $b \geq 3a$, since the peak of $w_2(r)/\rho_T$ increases greatly, the decrease in the peak of $w_1(r)/\rho_T$ can be ignored.

6.2.3 Velocity fields

As shown in the previous subsections, when the cosolvent density increases around the solute, c approaches the value of the stick boundary condition. The stick boundary condition means that the velocity is zero at the solute surface. Thus, the present results indicate that the high density makes the velocity small at the solute surface. In this subsection, I show that the velocity fields change depending on the cosolvent density around the solute. Furthermore, I discuss why the high density around the solute causes the stick boundary condition.

Figure 6.4 shows the barycentric velocity fields for $\phi_2 = 0.05$ at (a) $b = 2a$ and (b) $b = 6a$. The velocity are calculated using Eqs. (4.3) and (4.4), where c and d in Eqs. (4.3) and (4.4) are calculated from α and β given by Eqs. (5.61) and (5.63). Here, the velocity is assumed to be $u\hat{\mathbf{z}}$ at $r \to \infty$, where $\hat{\mathbf{z}}$ is the unit vector in the $\mathbf{z}$ direction. The velocity around the solute at $b = 6a$ is much smaller than that at $b = 2a$ (Fig 6.4). When $b = 6a$, the velocity almost vanishes near the solute surface. Note that the cosolvent density around the solute at $b = 6a$ is much higher than that of $b = 2a$.

Figure 6.5 shows the r dependence of the θ component of the velocity fields. When $b = 2a$, θ component of the velocity field is close to that assumed the slip boundary condition. In contrast, when $b = 6a$, the velocity field is in good agreement with that assumed the stick boundary condition. This result is consistent with the value

of c, which has a close value of the stick boundary condition at $b = 6a$.

From these results, the high density around the solute has a strong correlation with the stick boundary condition. This relation can be interpreted in terms of the slow motion of cosolvent spheres around the solute. The high density may result the slow motion of the cosolvent spheres because the cosolvent spheres cannot move easily in the crowded space, If the velocity is zero at the solute surface, the stick boundary condition holds. Thus, I consider that the increase in the density changes the boundary condition from the slip to the stick boundary conditions.

6.3 Summary and Discussion

Applying the perturbation theory, I have evaluated the boundary condition coefficient c of a large hard-sphere solute in binary hard-sphere mixtures. When the size ratio of binary mixtures is 2, c has close values of the slip boundary condition. In contrast, when the ratio is larger than 3, c approaches the stick boundary condition with adding the cosolvent spheres. I found the transition to the stick boundary condition when the peak of the cosolvent mass density increases around the solute. As the density of cosolvent spheres increases, the barycentric velocity around the solute approaches zero.

The present results for binary hard spheres are consistent with the previous studies of a one-component solvent with attractive interaction between solvent and solute particles.[21], [22], [29], [34] In a one-component solvent system, when the attractive force increases, the boundary condition changes from the slip boundary condition to the stick boundary condition. The attractive force causes the high density of the solvent around the solute. In the present binary hard-sphere system, the boundary condition also changes to the stick boundary condition with increasing the density around the solute. The present high density is caused not by the attractive force but by the entropic effect.

In this study, the radial distribution functions $g_i(r)$ are calculated using the HNC approximation, which is known to overestimate the peak value at the solute surface. I discuss the influence of the overestimate by the HNC approximation on c in Appendix A. I conclude that the transition to the stick boundary condition is not qualitatively affected by the approximation of the radial distribution functions.

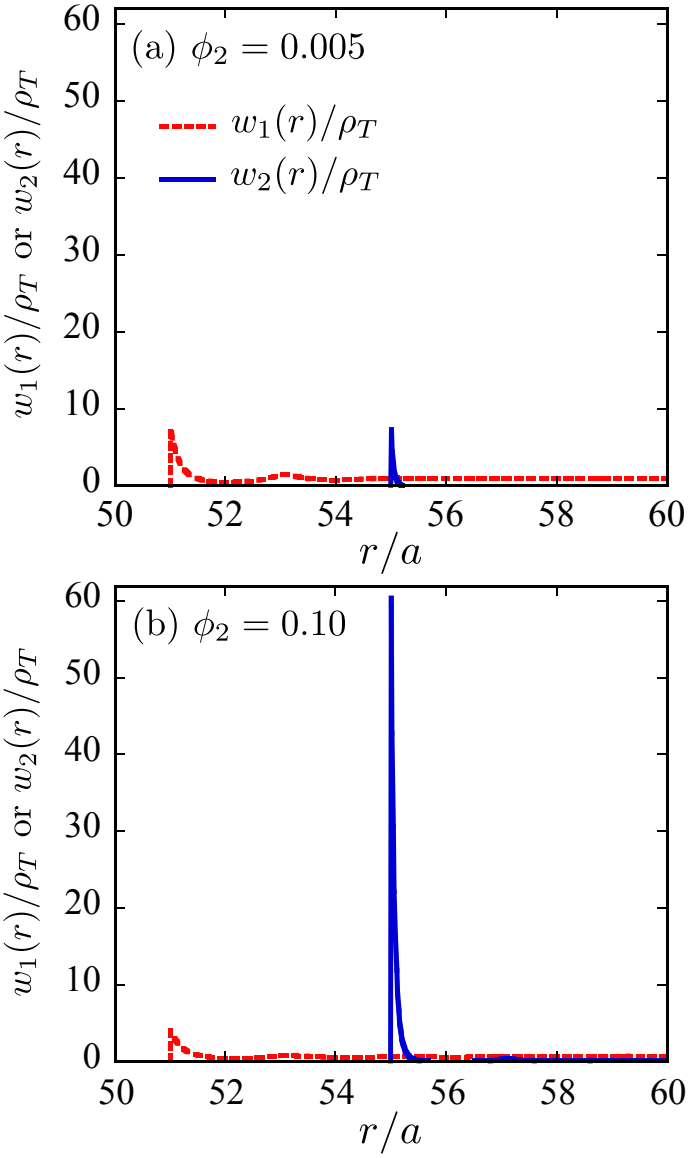

Figure 6.2 Reduced mass density fields of the solvent $w_1(r)/\rho_T$ and cosolvent $w_2(r)/\rho_T$ at the cosolvent size of $5a$. Here, ρ_T is the total bulk mass density and a is the radius of the solvent sphere. The dashed and solid curves represent the reduced mass density fields of the solvent and cosolvent spheres, respectively. The packing fractions of the cosolvent ϕ_2 are (a) 0.01 and (b) 0.10. The total packing fraction of the solvent and cosolvent is 0.38.

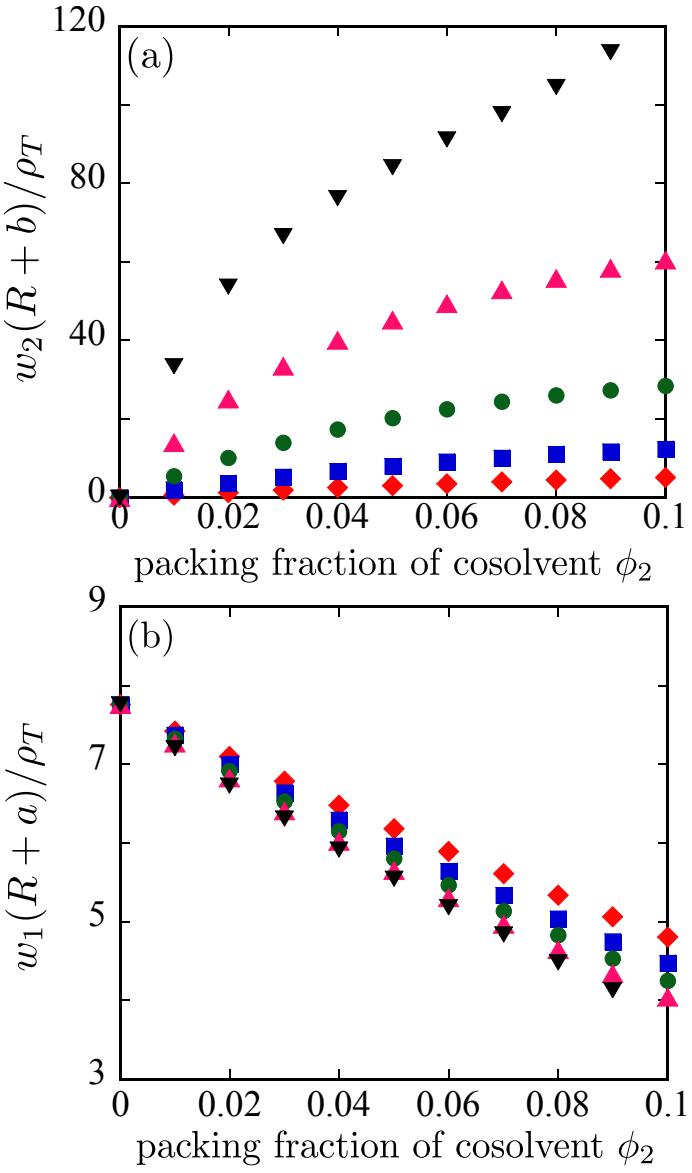

Figure 6.3 Mass densities of (a) cosolvent and (b) solvent at the solute surface, $w_2(R+b)$ and $w_1(R+a)$, respectively, for a binary hard-sphere system. Here, ρ_T is the total bulk mass density. The radius of the solute sphere is $50a$, where a is the radius of the solvent sphere. The radii of the cosolvent spheres b are $2a$ (diamonds), $3a$ (squares), $4a$ (circles), $5a$ (upward triangles), and $6a$ (downward triangles). The total packing fraction of the solvent and cosolvent is 0.38.

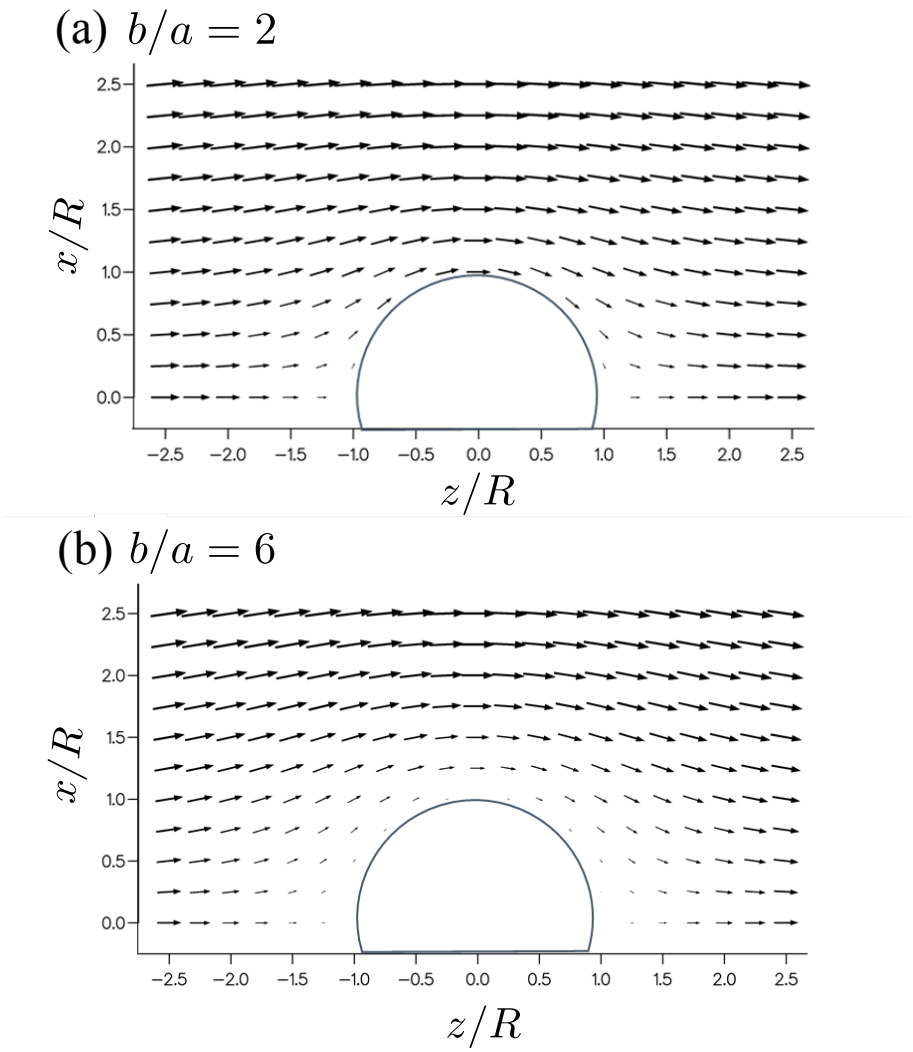

Figure 6.4 Barycentric velocity fields $\mathbf{v}(\mathbf{r})$ for $x \geq 0$ on the xz plane. The radii of the cosolvent sphere b are (a) $2a$ and (b) $6a$, respectively, where a is the radius of the solvent sphere. The radius of the solute sphere R is $50a$. The arrow direction represents the velocity direction and the length is proportional to the magnitude of the velocity. The solid curves represent the solute surface. The packing fraction of the cosolvent ϕ_2 is 0.05. The total packing fraction of the solvent and cosolvent is 0.38.

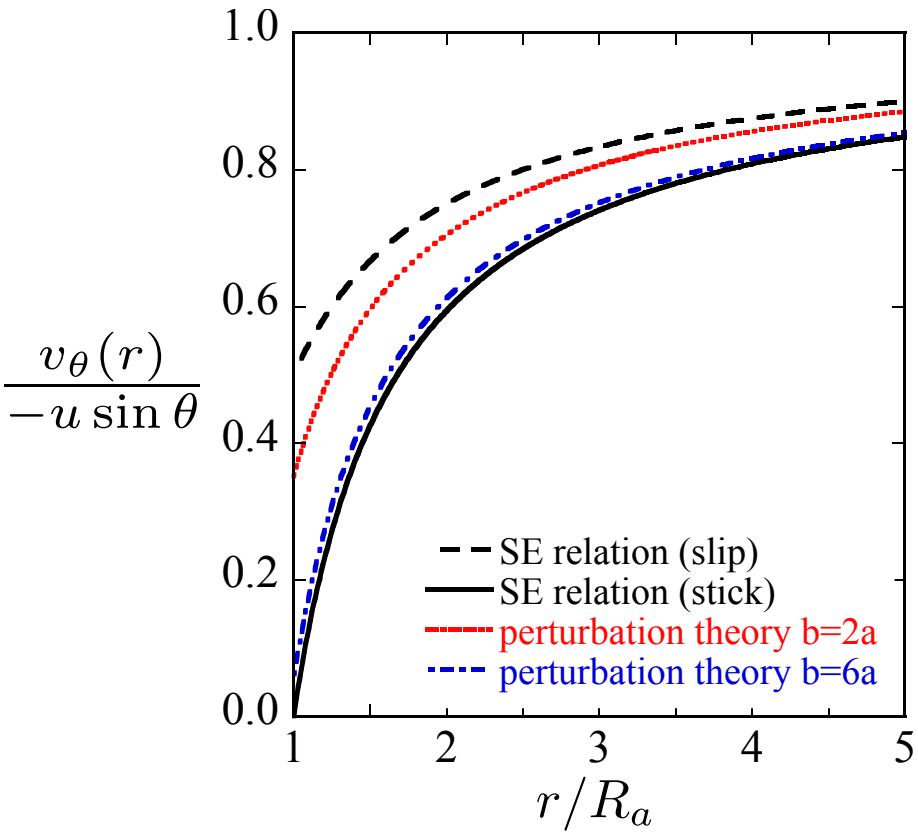

Figure 6.5 The r dependence of the θ component of the barycentric velocity fields $-v_\theta(r)/u\sin\theta = v_u(r)$. Here, $-v_\theta(r)/u\sin\theta = v_u(r)$ where $v_u(r)$ is given by Eqs. (4.3), which does not depends on θ. The dotted and dashed dotted curves represent the velocity calculated by the perturbation theory when the radii of the cosolvent sphere b are $2a$ and $6a$, respectively. The radius of the solute sphere R is $50a$. The dashed and solid cureves represent the velocity calculated assuming the slip and stick boundary condition, respectively. The packing fraction of the cosolvent ϕ_2 is 0.05. The total packing fraction of the solvent and cosolvent is 0.38.

Chapter 7

Conclusion

To clarify the solvation effect on the diffusion coefficient, a theory of a mobility in a one-component solvent system was formulated on the basis of the perturbation theory formulated by Inayoshi *et al.* They derived the drag coefficient up to the first order of the size ratio of solute and solvent particles. In contrast to the theory of Inayoshi *et al.*, I obtained the analytical expression of the drag coefficient including the terms higher than the second order. The comparisons with both the previous theory and MD simulations showed that the numerical results of the present theory agree well with those of previous studies at the large solute. Using this theory, one can calculate the diffusion coefficient of the large particle considering the solvation effect through the radial distribution functions. The present theory does not suffer from the finite-size effect.

The theory for the large particle mobility in a binary solvent mixture was also formulated by extending the perturbation theory of the one-component solvent system. From the perturbation expansion with respect to the size ratio of solute and solvent particles, it was shown that the boundary conditions on the solute surface are determined by the solvation structure of a binary mixture around the solute. Solving the hydrodynamic equations under the derived boundary conditions, the analytical expression of the drag coefficient was obtained. The drag coefficient can be calculated from the radial distribution function of a binary mixture without the finite-size effect.

Applying the present theory to a binary hard-sphere system, the boundary condition coefficient was evaluated for a large hard sphere solute. When a size ratio of binary solvent spheres is three or above, the boundary condition changes from the slip to stick boundary conditions as adding larger solvent spheres. The boundary condition changes when the solvent density around the solute increases. When the boundary condition changes from the slip to stick, the diffusion coefficient is reduced

to two-third.

The present study shows that the solvation structure can affect the diffusion of a large particle, especially in a multi-component system. Thus, the solvation structure is expected to affect the diffusion in a biological system. In the cytoplasm, biomolecules are immersed in a multi-component mixture including nucleic acids, glu- cides, and lipids. Actually, in vitro experiments on the protein diffusion have shown the deviation from the SE relation when adding cosolvent molecules.[5]–[8] One can consider that this deviation is caused by the solvation structure because the solvation effect is not included in the SE relation.

The study of various interaction systems will be a subject for future work. For instance, there are systems in which the cosolvent particles cannot approach the solute particle in contrast to the hard sphere system. This behavior is observed in some cosolvents, such as sucrose and polyethylene glycol, around the protein. The present perturbation theory can be applied not only to the hard sphere system but also to any spherical interaction system through the radial distribution functions. I consider that the application of the present theory to systems leads to the understanding of the diffusion behavior in biological systems.

Acknowledgement

I would like to express my sincere gratitude to Prof. Akira Yoshimori for his support and warm encouragement during the course of my study. His advice and comments were an enormous help to me. Special thanks go to Prof. Ryo Akiyama for constructive comments and discussion on my study. I would also like to thank him for the numerical calculation of the radial distribution functions. I owe my deepest gratitude to Prof. Tsuyoshi Yamaguchi of Nagoya University for his advice about formulating the theory. I would also like to thank Prof. Masahiro Kinoshita of Kyoto University for the software program used in the numerical preparation to obtain the radial distribution functions.

I would like to express the deepest appreciation to Prof. Hiizu Nakanishi and Prof. Yasuyuki Kimura who give me valuable comments and suggestions on my study. My heartfelt appreciation goes to Dr. Jun Matsui for his insightful comments on my study and presentation. I would also like to thank my colleagues of the condensed matter theory group at Kyushu University for their friendship and support.

Finally, I am deeply grateful to my family for their warm supports and encouragements.

This research was supported by the Japan Society for the Promotion of Science for a Research Fellowship (No. 25-4159).

Appendix A

Influence of HNC approximation

In Chap. 6, to calculate the diffusion coefficient c, I used the radial distribution functions $g_i(r)$ calculated by the HNC approximation. It is known that the HNC approximation overestimates the peak value at the solute surface.[46] Thus, I discuss the influence of the overestimate by the HNC approximation on c, using the different radial distribution functions which have more accurate peak values.

The peak values are obtained by the Boublik-Grundke-Henderson-Lee-Levesque (BGHLL) expression as[78]–[80]

$$g_i^{BGHLL}(R+r_i) = \frac{1}{1-\phi_T} + \frac{3}{(1-\phi_T)^2}\frac{Rr_i}{R+r_i}\left(\frac{\phi_1}{a}+\frac{\phi_2}{b}\right) + \frac{2}{(1-\phi_T)^3}\left\{\frac{Rr_i}{R+r_i}\left(\frac{\phi_1}{a}+\frac{\phi_2}{b}\right)\right\}^2, \tag{A.1}$$

where $r_1 = a$ and $r_2 = b$. In addition, ϕ_T, ϕ_1, and ϕ_2 are the total, solvent, cosolvent, packing fractions, respectively. The BGHLL expression is known to describe the peak values of $g_i(r)$ of hard sphere mixtures very well.

Using the peak values of the BGHLL expression, I obtain the radial distribution functions as

$$h_i(r) = \frac{h_i^{BGHLL}(R+r_i)}{h_i^{HNC}(R+r_i)} h_i^{HNC}(r) \qquad r \geq R+r_i, \tag{A.2}$$

where $h_i(r) = g_i(r) - 1$, and $h_i^{HNC}(r)$ is the correlation function obtained by the HNC approximation. Although $g_i(r)$ given by Eq. (A.2) has a peak value of the BGHLL expression, $g_i(r)$ is not improved elsewhere.

Figure A.1 shows the peak value of $w_2(R+b)/\rho_T$ and $w_1(R+b)/\rho_T$ calculated by Eq. (A.1). The peak of $w_2(R+b)/\rho_T$ increases with the cosolvent packing fraction and cosolvent sphere radius. The peak of $w_1(R+b)/\rho_T$ decreases with increasing cosolvent packing fraction and cosolvent sphere radius. These behavior are the

same as observed in the results of the HNC approximation (Fig. 6.3). However, the absolute value of the peaks are much smaller than those of the HNC approximation. For instance, the value of $w_2(R+b)/\rho_T$ given by the BGHLL expression is a eighth less than that of the HNC approximation when $b = 5a$ at $\phi_2 = 0.01$.

I calculate the boundary condition coefficient c using $g_i(r)$ given by Eq. (A.2) (Fig. A.2). The calculated results show that c approaches the value of the stick boundary condition with increasing the cosolvent sphere radius. Although values of c are smaller than those obtained by the HNC approximation, it is expected that the stick boundary condition holds at a size ratio larger than 6. Thus, I conclude that the transition to the stick boundary condition is not qualitatively affected by the approximation of the radial distribution functions. In order to obtain quantitatively accurate values of c, however, one needs to improve $g_i(r)$ everywhere by methods such as Monte Carlo simulations or more accurate approximation.

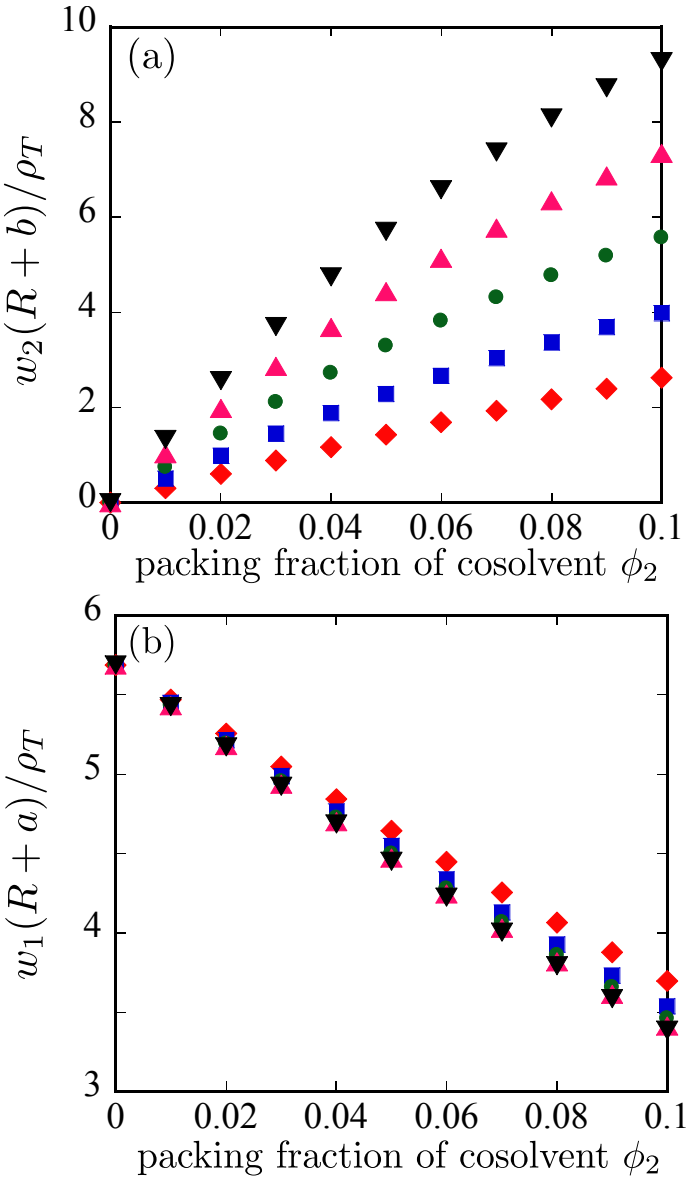

Figure A.1 Mass densities of (a) cosolvent and (b) solvent at the solute surface, $w_2(R+b)$ and $w_1(R+a)$, respectively, for a binary hard-sphere system. The peak values of $g_i(r)$ are obtained using Eq. (A.1). Here, ρ_T is the total bulk mass density and R, a, and b are the radii of solute, solvent, and cosolvent spheres, respectively, The symbols are the same as those in Fig. 6.1.

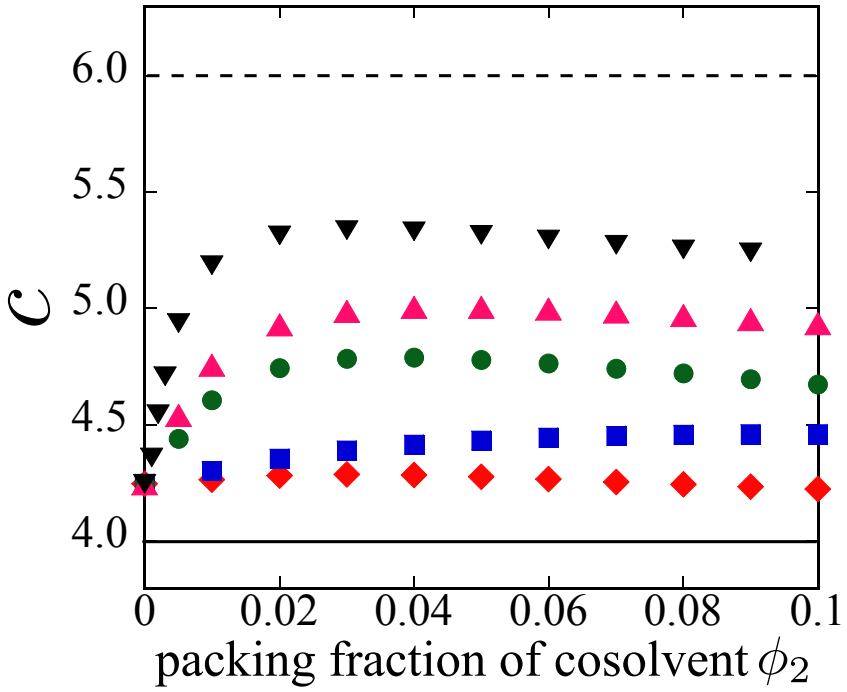

Figure A.2 Dependence of the boundary condition coefficient c on the packing fraction of cosolvent spheres ϕ_2. The radial distribution functions $g_i(r)$ are obtained using Eq. (A.2). The symbols are the same as those in Fig. 6.1.

Bibliography

[1] S. Nishida, T. Nada, and M. Terazima, Biophys. J. **87**, 2663 (2004).

[2] S. Nishida, T. Nada, and M. Terazima, Biophys. J. **89**, 2004 (2005).

[3] J. S. Khan, Y. Imamoto, M. Harigai, M. Kataoka, and M. Terazima, Biophys. J. **90**, 3686 (2006).

[4] A. Bonincontro, V. Calandrini, and G. Onori, Colloids Surf. B: Biointerfaces **21**, 311 (2001).

[5] T. Yoshitake and M. Terazima, private communications

[6] S. Zorrilla, M. A. Hink, A. J. W. G. Visser, and M. P. Lillo, Biophys. Chem. **125**, 298 (2007).

[7] B. Varga, F. Migliardo, E. Takacs, B. Vertessy, S. Magazù, and C. Mondelli, Chem. Phys. **345**, 250 (2008).

[8] M. Iwaki and T. Yanagida, presented at Int. Symp. Hydration and ATP Energy, 2010.

[9] R. Castillo, C. Garza, and S. Ramos, J. Phys. Chem. **98**, 4188 (1994).

[10] H. E. Smorenburg, R.M. Crevecoeur, I. M. de Schepper, and L. A. de Graaf, Phys. Rev. E **52**, 3 (1995).

[11] C. Lederle, W. Hiller, C. Gainaru, and R. Böhmer, J. Chem. Phys. **134**, 064512 (2011).

[12] G. D. J. Phillies, J. Phys. Chem. **85**, 2838 (1981).

[13] T.-H. Lin and G. D. J. Phillies, Macromolecule **17**, 1686 (1984).

[14] G. H. Koenderink, S. Sacanna, D. G. A. L. Aarts, and A. P. Philipse, Phys. Rev. E **69**, 021804 (2004).

[15] B. Alberts, D. Bray, J. Lewis, M. Raff, K. Roberts, and J. D. Watson, *Molecular biology of the cell*, 5th ed. (Garland Publishing, New York, 2008).

[16] D. S. Goodsell, *The Machinery of Life*, 2nd ed. (Springer, New York, 2009).

[17] L. D. Landau and E. M. Lifshitz, *Fluid Mechanics* (Butterworth-Heinemann, Oxford, U.K., 1987).

[18] H. J. V. Tyrrell and K. R. Harris, *Diffusion in Liquids* (Butterworths, London, 1984).

[19] D. F. Evans, T. Tominaga, and C. Chan, J. Solution Chem. **8**, 461 (1979).

[20] D. F. Evans, T. Tominaga, and H. T. Davis, J. Chem. Phys. **74**, 1298 (1981).

[21] R. Biswas, S. Bhattacharyya, and B. Bagchi, J. Phys. Chem. B **102**, 3252 (1998).

[22] G. Srinivas, S. Bhattacharyya, and B. Bagchi, J. Chem, Phys **110**, 4477 (1999).

[23] S. Bhattacharyya, and B. Bagchi, J. Chem. Phys. **106**, 1757 (1997).

[24] S. Bhattacharyya, Chem. Phys. Lett. **386**, 83 (2004).

[25] S. A. Egorov, J. Chem. Phys. **134**, 084903 (2011).

[26] T. Yamaguchi, T. Matsuoka, and S. Koda, J. Chem. Phys. **123**, 034504 (2005).

[27] T. Yamaguchi, T. Matsuoka, and S. Koda, J. Mol. Liq. **134**, 1 (2007).

[28] R. O. Sokolovskii, M. Thachuk, and G. N. Patey, J. Chem. Phys. **125**, 204502 (2006).

[29] J. R. Schmidt and J. L. Skinner, J. Phys. Chem. B **108**, 6767 (2004).

[30] S. H. Lee, Theor. Chem. Acc. **127**, 613 (2010).

[31] J. R. Schmidt and J. L. Skinner, J. Chem. Phys. **119**, 8062 (2003).

[32] Z. Li, Phys. Rev. E **80**, 061204 (2009).

[33] F. Ould-Kaddour and D. Levesque, Phys. Rev. E **63**, 011205 (2000).

[34] J. Liu, D. Cao, and L. Zhang, J. Phys. Chem. C **112**, 6653 (2008).

[35] M. Sharma and S. Yashonath, J. Phys. Chem. B **110**, 17207 (2006).

[36] T. Yamaguchi and Y. Kimura, Mol. Phys. **98** 1553 (2000).

[37] O. Kravchenko and M. Thachuk, J. Chem. Phys. **134**, 114310 (2011).

[38] M. Cappelezzo, C. A. Capellari, S. H. Pezzin, and L. A. F. Coelho, J. Chem. Phys. **126**, 224516 (2007).

[39] M. Fushiki, Phys. Rev. Lett. **68**, 021203 (2003).

[40] Y. Inayoshi, A. Yoshimori, and R. Akiyama, J. Phys. Soc. Jpn. **81**, 114603 (2012).

[41] A. Einstein, Ann. Phys. **19**, 371 (1906).

[42] G. I. Taylor, Proc. R. Soc. London, Ser. A **219**, 186 (1953).

[43] P. A. Heiney, Phys. Rev. Lett. **22**, 2911 (1991).

[44] M. Terazima and N. Hirota, J. Chem. Phys. **98**, 6257 (1993).

[45] E. Chen, P. Wittung-Stefshede, and D. S. Kliger, J. Am. Chem. Soc. **121**, 3811 (1999).

[46] J. P. Hansen and I. R. McDonald, *Theory of Simple Liquids* (Academic Press, London, 1986).

[47] U. Balucani and M. Zoppi, *Dynamics of the Liquid State* (Clarendon, Oxford, 1994).

[48] B. J. Alder, W. E. Alley, and J. H. Dymond, J. Chem. Phys. **61**, 1415 (1974).

[49] J. J. Erpenbeck and W. W. Wood, Phys. Rev. A **32**, 412 (1985).

[50] J. R. Mehaffey and R. I. Cukier, Phys. Rev. A **17**, 1181 (1978).

[51] B. J. Alder, W. M. Gass, and T. E. Wainwright, J. Chem. Phys. **53**, 3813 (1970).

[52] J. R. Mehaffey and R. I. Cukier, Phys. Rev. Lett. **38**, 1039 (1977).

[53] L. Sjoögren and A. Sjolander, J. Phys. C **12**, 4369 (1979).

[54] T. R. Kirkpatrick and J. C. Nieuwoudt, Phys. Rev. A **33** 2651 (1986).

[55] T. R. Kirkpatrick and J. C. Nieuwoudt, Phys. Rev. A **33**, 2658 (1986).

[56] J. R. Mehaffey and R. I. Cukier, Phys. Rev. Lett. **38** 1039 (1977).

[57] H. Mori, Prog. Theor. Phys. **33**, 423 (1965).

[58] T. Munakata, *Butsuri Tokeigaku* (Asakura, Tokyo, 1996) [in Japanese].

[59] H. Fujisaka, *Hiheikoukei no Tokei Rikigaku* (Sangyo Tosyo, Tokyo, 1998) [in Japanese].

[60] S. W. Lovesey, J. Phys. C **4**, 3057 (1971).

[61] S. A. Egorov, J. Chem. Phys. **119**, 4798(2003).

[62] S. P. Das and G. F. Mazenko, Phys. Rev. A **34**, 2265 (1986).

[63] B. Sen Gupta, S. P. Das, and J.-L. Barrat, Phys. Rev. E **83**, 041506 (2011).

[64] B. Sen Gupta and S. P. Das, J. Chem. Phys. **136**, 154506 (2012).

[65] M. Shibata, *Zenkin Kyusu to Tokui Setsudouhou* (Morikita, Tokyo, 2009) [in Japanese].

[66] M. Kinoshita and M. Harada, Mol. Phys. **74**, 443 (1991).

[67] M. Kinoshita and M. Harada, Mol. Phys. **79**, 145 (1993).

[68] M. Kinoshita and M. Harada, Mol. Phys. **81**, 1473 (1994).

[69] M. Kinoshita and D. Berard, J. Comput. Phys. **124**, 230 (1996).

[70] M. Kinoshita, S. Iba, K. Kuwamoto, and M. Harada, J. Chem. Phys. **105**, 7177 (1996).

[71] M. Kinoshita, Y. Okamoto, and F. Hirata, J. Comput. Chem. **19**, 1724 (1998).

[72] Y. Karino, R. Akiyama, and M. Kinoshita, J. Phys. Soc. Jpn. **78**, 044801 (2009).

[73] Y. Nakamura, A. Yoshimori, and R. Akiyama, J. Phys. Soc. Jpn. **81**, SA026 (2012).

[74] Y. Nakamura, A. Yoshimori, and R. Akiyama, J. Phys. Soc. Jpn. **83**, 064601 (2014).

[75] Y. Nakamura, A. Yoshimori, and R. Akiyama, J. Mol. Liq. **200**, 85 (2014).

[76] K. Miyazaki, K. Kitahara, and D. Bedeaux, Physica A **230**, 600 (1996).

[77] K. Kitahara, *Hiheikokei no Tokei Rikigaku* (Nonequilibrium Statistical Physics) (Iwanami, Tokyo, 1997) [in Japanese].

[78] T. Boublík, J. Chem. Phys. **53**, 471 (1970).

[79] E. W. Grundke and D. Henderson, Mol. Phys. **24**, 269 (1972).

[80] L. L. Lee and D. Levesque, Mol. Phys. **26**, 1351 (1973).